Parametric analysis of carbon nanofiber effects on mechanical properties and abrasion resistance of GF/PPS hybrid composites

Arun Y C, Ravishankar R, Suresha B, Pradeep Kumar V G, Tejas M R
Department of Mechanical Engineering, Sri Jayachamarajendra College of Engineering, JSS Science and Technology University, Mysuru -570006, Karnataka, India
arunyc@jssstuniv.in, http://orcid.org/0009-0009-4682-8392
ravishankar.r@jssstuniv.in, http://orcid.org/0000-0003-4503-7686
sureshab@jssstuniv.in, http://orcid.org/0009-0005-3230-0264
pvg@jssstuniv.in, http://orcid.org/0009-0003-9690-8127
mrtejas@jssstuniv.in, http://orcid.org/0009-0007-7266-4585

ABSTRACT. The focus of this research was to investigate the effects of carbon nanofiber (CNF) reinforcement on the mechanical performance, interfacial characteristics, and abrasive wear behavior of short glass fiber/polyphenylene sulfide (GF/PPS) hybrid nanocomposites intended for high-performance tribological applications. Melt processing was used to fabricate GF/PPS hybrid nanocomposites with 0, 0.4, and 0.8 wt% CNFs, which were then methodically characterized. Through π–π interactions between CNFs and the polymer matrix, FTIR measurements demonstrated enhanced interfacial compatibility while confirming the retention of the PPS chemical structure. The addition of CNFs demonstrated improved fiber–matrix adhesion and load transmission capability by increasing composite density, decreasing void content, and considerably improving interlaminar shear strength (23.7%) and hardness (20%). Studies on two-body abrasive wear showed significant decreases in wear loss and coefficient of friction (CoF), with the 0.8 wt% CNF-filled composite showing the best tribological performance because a stable and continuous lubricating tribo-film was formed. Applied load mostly controlled the CoF behavior, while sliding velocity and abrasive grit size primarily affected wear loss, according to statistical ANOVA data. With prediction errors under 6.5% and coefficient of determination (R^2) values between 73% and 77%, regression models demonstrated strong predictive power. The change from severe micro-cutting, matrix deterioration, and fiber pull-out in unfilled composites to mild ploughing and protective tribo-layer development in CNF-reinforced composites was further validated by worn surface morphology. The CNF modified GF/PPS hybrid nanocomposites are promising materials for automotive transmission components, bearing cages, thrust washers, gears, and power plant chute liners operating under extreme abrasive wear conditions, as evidenced by the synergistic improvement in mechanical strength, interfacial bonding, and tribological stability.

KEYWORDS. Glass fiber reinforced PPS composites, Carbon nanofibers, Mechanical properties, Taguchi method, Abrasive wear, Worn surface morphology.

Citation: Arun, Y C, Ravishankar, R, Suresha, B, Pradeep Kumar, V G, Tejas, M R., Parametric Analysis of Carbon Nanofiber Effects on Mechanical Properties and Abrasion Resistance of GF/PPS Hybrid Composites, Fracture and Structural Integrity, 77 (2026) 316-339.

Received: 30.03.2026
Accepted: 22.05.2026
Published: 25.05.2026
Issue: 07.2026

Copyright: © 2026 This is an open access article under the terms of the CC-BY 4.0, which permits unrestricted use, distribution, and reproduction in any medium, provided the original author and source are credited.

INTRODUCTION

The use of high-performance polymer matrix composites, especially those based on polyphenylene sulfide (PPS), in tribological components is growing because of their superior chemical resistance, thermal stability, and intrinsic dimensional integrity in harsh working conditions. Glass fiber-reinforced PPS (GF/PPS) composites are frequently used in structural and seafaring applications where mechanical loads and resistance to corrosive environments are crucial [1, 2]. However, their tribological performance continues to be a major factor limiting service life and dependability, particularly in abrasive situations involving hard counter face or trapped particles [3, 4].

Abrasive wear in polymer composites is a complicated surface degradation event that involves third-body interactions, fatigue-induced delamination, microcutting, and microploughing. The mechanical integrity of the composite surface, contact pressure, and the size of the abrasive grit all significantly influence the wear severity in two-body abrasion. Recent research has shown that the development of stable transfer films and the capacity of reinforcements to support applied loads without interfacial failure are closely related to the wear resistance of PPS-based composites. For example, adding PTFE and other solid lubricants to GF/PPS composites encourages the development of low-shear transfer layers, which minimizes surface damage and reduces direct asperity contact [5]. Similarly, it has been claimed that inorganic nanoparticle reinforcements reduce wear and friction by creating compact protective tribo-films and micro-bearing effects [6].

The ability of carbon-based reinforcements to simultaneously enhance the mechanical and tribological performance of polymer composites has attracted a lot of attention. Carbon fibers (CFs), carbon nanotubes (CNTs), and carbon nanofibers (CNFs) influence wear mechanisms and frictional behavior by improving load transmission, fracture resistance, and heat conductivity. The crucial importance of interfacial chemistry has been further highlighted by recent research on surface-modified CF/PPS composites, where improved fiber–matrix adhesion results in lower wear rates, better load-bearing capacity, and increased stability of transfer films under sliding conditions [7].

The substantial potential of nanoparticle-reinforced polymer composites for improved mechanical and surface properties has been shown in earlier research. Using an RVE-based finite element method, Sahu and Sreekanth observed increased stiffness and stress-bearing capacity in HDPE composites loaded with nanodiamonds [8]. In a similar vein, Sahoo et al. [9] found improved mechanical performance in graphene-reinforced polyurethane composites, and simulation and experimental results agreed well. In HDPE hybrid composites reinforced with MWCNTs and h-BNNPs, Badgayan et al. demonstrated enhanced wetting behavior, highlighting the impact of surface shape and nanoparticle reinforcement [10]. Furthermore, research on hybrid polymer composites augmented with nano-fillers shows that even little nanomaterial additions can greatly increase abrasion resistance by strengthening interfacial adhesion and limiting plastic deformation under sliding conditions [11].

Carbon nanofibers offer distinct advantages over other nano-reinforcements due to their high aspect ratio, graphitic structure, and ability to form linked networks within a polymer matrix [12–14]. These nanofibers improve hardness and prevent surface deterioration under abrasive loading by limiting the mobility of polymer chains and stopping cracks. Additionally, they restrict direct material removal at the sliding interface by forming a protective carbonaceous tribo-layer [12, 13]. However, the dispersion, loading percentage, and interaction of CNFs with the primary fiber reinforcement have a significant impact on their effectiveness, particularly in hybrid systems such as GF/PPS composites. While different nanofillers (such as graphene, nanoclay, MoS_2, and cellulose nanofibers) greatly increase abrasion resistance by strengthening interfacial bonding, their effectiveness is strongly influenced by operating parameters like applied load, sliding distance, and abrasive grit size, according to recent studies (Tab. 1). The wear behavior is usually shifted toward severe material removal dominated by micro-cutting with coarser grits. Systematic study is still lacking, despite the fact that hybrid reinforcement systems (fiber + nanofiller) can use synergistic effects to lessen this severity, changing the major wear mechanism from micro-cutting to moderate micro-ploughing. In particular, there aren't many thorough studies assessing CNF-reinforced PPS composites under two-body abrasive wear circumstances with different abrasive grit sizes [11, 14–27].

The fact that abrasive wear of polymer composites is controlled by the combined influence of material qualities (such as hardness and interfacial strength) and operational factors (such as load, abrasive grit, and sliding distance) rather than a single element is a crucial part of tribological investigations. Response Surface Methodology (RSM) and Taguchi procedures are two statistical design approaches that have been shown to be useful in finding dominating elements and their interactions in multi-parameter systems [28]. Nevertheless, there is still little use of these multi-level designs (L27 orthogonal array) in CNF-modified GF/PPS composites. Additionally, recent studies (2024–2025) show that surface integrity and microstructural stability during repeated sliding have a significant impact on abrasive wear resistance in hybrid composites. In advanced composite systems, the impact of filler synergy and reinforcement architecture on wear mechanisms such as tribo-layer evolution, debris compaction, and groove formation has been extensively documented [29]. These results highlight the necessity of a thorough parametric study that connects tribological performance to abrasive conditions, hardness, and nano-reinforcement.

Composite System	Nanofiller /Filler	Abrasive Medium (Grit)	Key Findings	Refs.
CF/PA6 + TPC hybrid	Silane-treated graphene + SiO_2 (0–3 wt%)	SiC emery paper (320 grit)	Hybrid nanofillers significantly reduced specific wear rate (SWR); optimal 1.5% each filler improved interfacial bonding and abrasion resistance.	[11]
PA66/PA6 blend composites	PTFE + MoS_2	SiC paper (180 grit)	PTFE-based systems showed improved wear resistance due to lubricating film; wear strongly dependent on load.	[19]
TCE + SGF + CF hybrid	PTFE, SiC, Al_2O_3	SiC abrasive paper	Multi-phase hybridization enhances wear resistance; filler combination governs micro-cutting vs micro-ploughing mechanisms.	[20]
Glass/Bamboo + nanoclay epoxy	Nanoclay	SiC abrasive	Nanoclay improved interfacial bonding and reduced wear; ANN/RSM confirmed significant reduction in SWR.	[21]
Basalt/abaca hybrid polymer composites	---	SiC paper (~320 grit)	Basalt fiber improved abrasion resistance over natural fibers; wear influenced by load & speed.	[22]
Cellulose nanomaterial composites	Cellulose nanofibers	Abrasion conditions	Nanocellulose improved surface hardness and wear resistance via strong interfacial network.	[23]
Carbon fabric epoxy	Graphite filler	SiC paper (150 & 320 grit)	Graphite reduced wear via solid lubrication and transfer film formation.	[24]
Carbon fiber epoxy + MoS_2	MoS_2 nanoparticles (0.1–0.7 wt%)	ASTM G99 (SiC abrasion conditions)	0.7 wt% MoS_2 reduced two-body wear (~18%) due to lubricating tribofilm and improved load sharing.	[25]
Hybrid fiber polymer composites (review with experiments)	Various nano-fillers	Abrasive wear conditions	Nanofillers reduce wear by forming protective tribolayers and enhancing stiffness (Nature)	[26]
PBI/HDPE composites	hybrid reinforcement	SiC abrasive	Wear strongly dependent on load and sliding distance; thermoplastic matrix showed improved ductile wear response.	[27]

Table 1: Recent literature on two-body abrasive wear behavior of fiber-reinforced thermoplastic/polymer composites with nanofillers.

This work is novel because it employs a Taguchi L27 design technique to systematically investigate CNF-reinforced GF/PPS hybrid composites under multi-pass two-body abrasive wear conditions with different SiC abrasive grit sizes. In contrast to previous research, the current study uses statistical optimization and mechanistic analysis to determine a relationship between nanofiller reinforcement, hardness, interlaminar shear strength, and abrasive wear performance.
The main goals of this work are to produce GF/PPS hybrid composites reinforced with CNF with different filler loadings and to systematically assess their hardness, interlaminar shear strength, and two-body abrasive wear performance. Additionally, the study intends to optimize the wear parameters using a Taguchi-based statistical design methodology for better wear resistance and surface durability, as well as examine the combined effects of applied load, sliding velocity, abrading distance, abrasive grit size, and CNF content on tribological behavior. The design and optimization of high-performance PPS-based hybrid composites for demanding tribological applications, especially in marine, automotive, and other severe wear-prone engineering settings, are anticipated to benefit from the study's findings.

MATERIALS AND METHODS

Materials

The matrix material was polyphenylene sulfide (PPS), which has remarkable mechanical strength, chemical resistance, and thermal stability. Being a semi-crystalline thermoplastic, PPS has good dimensional stability, low moisture absorption, and intrinsic flame retardancy, all of which hold true at high temperatures. The usual density, melting temperature, and tensile strength of commercial PPS granules (Padmini Innovative Marketing Solutions Pvt Ltd., Mumbai, India) are 1.34–1.36 g/cm³, 280–290 °C, and 70–90 MPa, respectively. A sterically hindered phenolic antioxidant (PETBP), which scavenges free radicals and reduces degradation, was added to enhance thermo-oxidative stability during processing.
The main reinforcement was made of short glass fibers (GFs), which have outstanding mechanical performance, are inexpensive, and are simple to produce. The fibers' high aspect ratio (length 6 mm, diameter 12 μm) allows for homogeneous dispersion and effective stress transfer inside the PPS matrix. Fine Organics (Mumbai, India) provided

commercial E-glass fibers, assuring uniform quality and compatibility. Strength and thermal stability are enhanced by their normal composition, which consists of SiO_2 (52–56 wt%), $Al2O_3$ (12–15 wt%), and CaO (21–23 wt%).

To improve mechanical, thermal, and interfacial properties, carbon nanofibers (CNFs) were used as nanoscale reinforcement. Aritech Chemazone Pvt Ltd. (India) offered the CNFs (diameter 30–45 nm, length >80 µm), which have a high aspect ratio, tensile strength (2–7 GPa), and modulus (200–600 GPa). Strong interfacial bonding is encouraged by their huge surface area, while wear resistance and heat dissipation are enhanced by their high conductivity and thermal stability (>600 °C).

PPS granules, CNFs, and GFs are the basic materials utilized in this investigation, as illustrated in Fig. 1. The SEM morphology of CNFs shown in Fig. 2 confirms their high aspect ratio by revealing a fibrous and entangled tubular structure. For efficient load transfer and reinforcement in polymer matrices, such morphology is beneficial. According to Energy-dispersive X-ray spectroscopy (EDAX) analysis presented in Fig. 3, CNFs have a low oxygen content and a high carbon purity, making them appropriate for use in nanocomposite applications.

Figure 1: Photographs of (a) PPS granules, (b) SGFs, (c) CNFs.

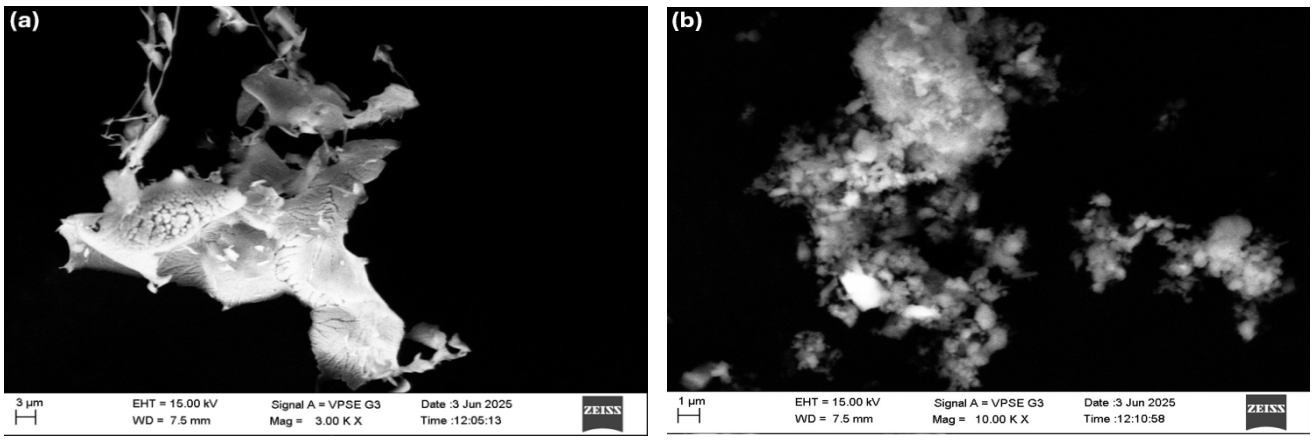

Figure 2: Microstructure of carbon nanofibers (a) 3 kX, (b) 10 kX.

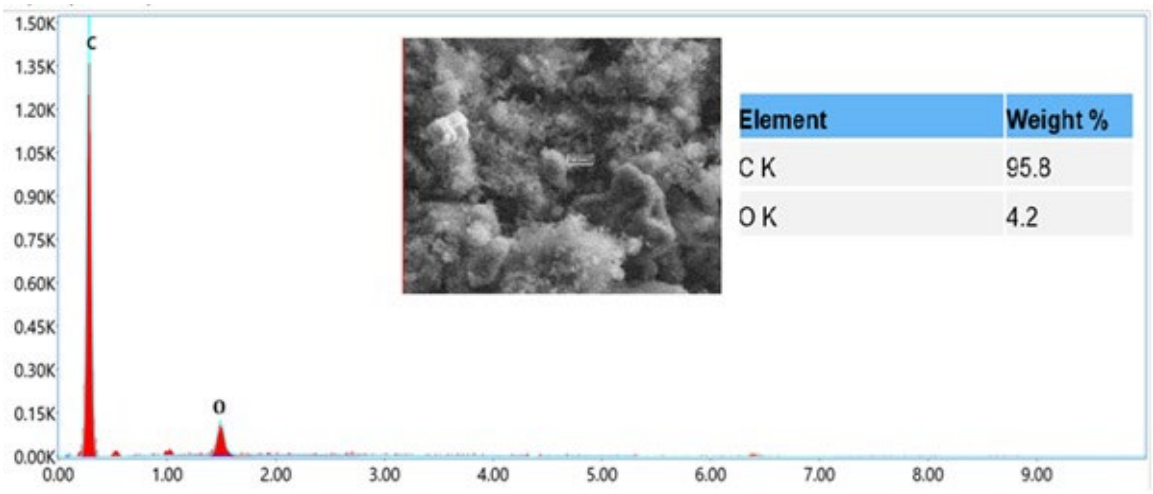

Figure 3: Energy-dispersive X-ray spectroscopy of carbon nanofibers.

Fabrication of GF/PPS/CNF Hybrid Nanocomposites

Fig. 4 shows the sequential multi-stage method used to fabricate the GF/PPS/CNF hybrid nanocomposites, which included drying, melt-compounding, and injection molding. The PPS pellets, GFs, and CNFs were first dried in a Hot Air Oven at 120°C for 6–8 h to ensure ideal interfacial bonding and avoid hydrolytic breakdown. After drying, the components were combined in a mechanical mixer before being put into a twin-screw extruder. The extruder barrel was kept at a progressive temperature profile between 290°C and 330°C because PPS has a high melting point of 280°C. For the homogeneous dispersion of CNFs and the wetting of GFs, this heat gradient promises sufficient melt viscosity. Composite pellets were produced by passing the resultant extrudate through a palletizer. To prepare standardized test samples, these pellets were then placed into an injection molding machine. To promote secondary crystallization and guarantee the dimensional stability of the PPS matrix, the injection barrel was kept between 300°C and 340°C, while the mold temperature was crucially maintained at 140°C.

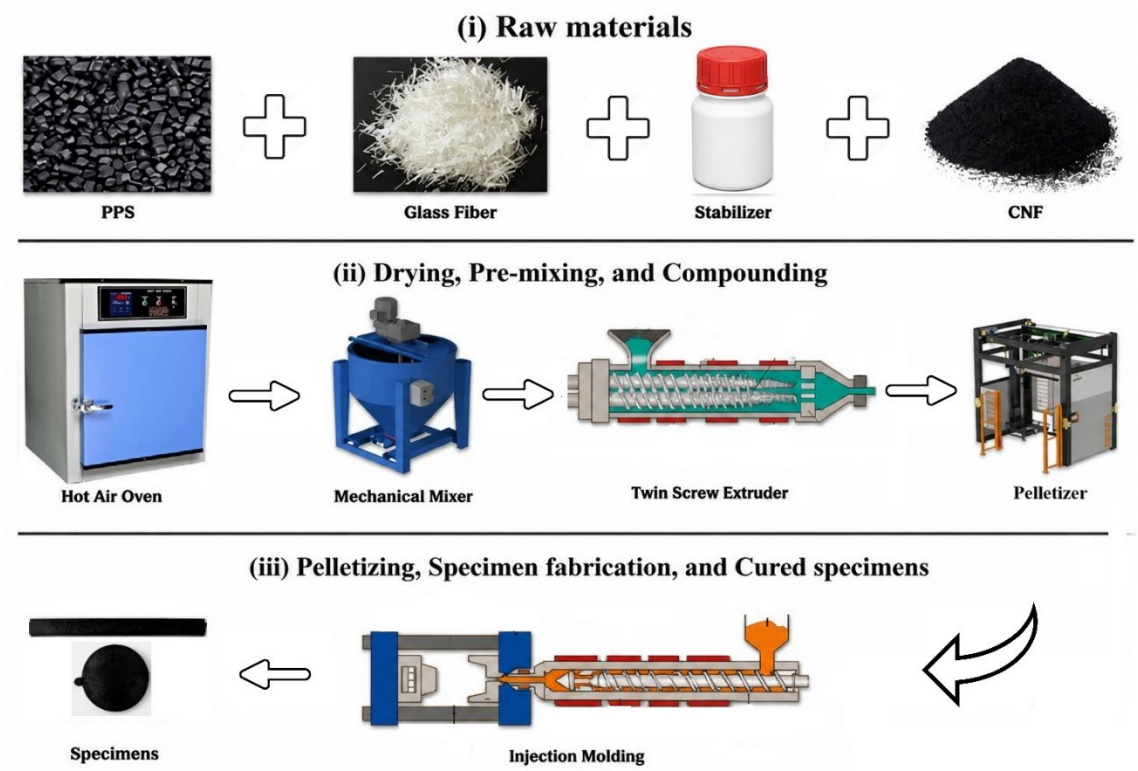

Figure 4: Schematic representation of composite fabrication and specimen preparation process: (i) raw materials, (ii) drying, pre-mixing, and compounding, and (iii) pelletizing, specimen fabrication, and cured specimens.

Tab. 2 shows that the fabrication process begins with a pre-treatment at 120°C to eliminate moisture and then melt-blending at temperatures as high as 330°C to achieve the best CNF dispersion. To ensure optimal crystallinity and structural integrity of the PPS matrix, the injection molding process ends at a high mold temperature of 135°C to 150°C.

Processing Stage	Equipment/Zone	Temperature (°C)	Duration
Pre-treatment	Hot Air Oven	120	6–8 h (moisture removal)
Compounding	Extruder Feed Zone	280 – 290	prevents premature melting
Melt Blending	Extruder Mixing Zones	310 – 330	ensures CNF dispersion
Molding	Injection Barrel/Nozzle	300 – 340	optimizes melt flow
Crystallization	Mold Temperature	135 – 150	promotes high crystallinity

Table 2: Thermal parameters for fabrication of GF/PPS/CNF hybrid nanocomposites.

The specific compositions of the produced hybrid nanocomposites, including different ratios of PPS, GFs, and CNFs, are summarized in Tab. 3. To assess the impact of different CNF loading on hardness, interlaminar shear strength and 2 BAW behavior of GF/PPS composites, the composite formulation was fabricated based on a thorough review of the literature and processing viability. This method makes it possible to systematically evaluate how reinforcement affects tribo-mechanical performance.

Composites	Codes	PPS (wt%)	SGFs (wt%)	CNFs (wt%)
GF+PPS	C0	60	40	---
GF+PPS+ 0.4 wt% CNF	C1	59.6	40	0.4
GF+PPS+ 0.8 wt% CNF	C2	59.2	40	0.8

Table 3: Constituents of GF/PPS/CNF hybrid nanocomposites.

Characterization - Fourier Transform Infrared Spectroscopy

Fourier Transform Infrared Spectroscopy (FTIR) was used to examine the chemical functional groups and interfacial interactions of the pure PPS, Glass Fiber (GF), and CNF-modified GF/PPS composites (C0, C1, and C2). A Bruker Alpha spectrometer fitted with an Attenuated Total Reflectance (ATR) accessory was used to record the spectra. To ensure a high signal-to-noise ratio, samples were scanned over a wavenumber range of 4000 to 500 cm^{-1} at a resolution of 4 cm^{-1}, with an average of 32 scans per sample. Samples were cleaned and dried before analysis to remove interference caused by moisture in the 3200–3600 cm^{-1} range.

Characterization - Density measurement and voids

Using the Archimedes' buoyancy method, the density of the produced hybrid nanocomposites was calculated in accordance with ASTM D792 [27]. A density kit-equipped METTLER AE 200 analytical balance was used for the measurements. The 100 mm diameter injection-molded discs were used to precisely slice test specimens (25 mm × 10 mm × 3.2 mm). Each composite series was tested twice, and the mean values were reported to ensure statistical repeatability and reliability.

The density testing parameters for the fabricated CNF-modified PPS composites are summarized in Tab. 4. These characteristics, which included the standard followed and specimen dimensions, were strictly adhered to ensure measurement reproducibility.

Parameter	Specification
Standard	ASTM D792 (Archimedes' Principle)
Equipment	METTLER AE 200 Analytical Balance
Specimen dimensions	25 mm × 10 mm × 3.2 mm
Source Material	100 mm diameter molded discs

Table 4: Density testing parameters for GF/PPS/CNF hybrid nanocomposites.

Using Eqs. (1) and (2), the theoretical composite density (ρ_t) and the empirically determined density were compared to get the void content (V_v).

$$\rho_t = \frac{1}{(W_f / \rho_f) + (W_m / \rho_m) + (W_{pf} / \rho_{pf})} \tag{1}$$

where, W_f, W_m and W_{pf} are wt% of fiber, matrix and particulate filler respectively. ρ_f, ρ_m and ρ_{pf} are density of fiber, matrix and particulate filler respectively.

$$V_v = \frac{\rho_{ct} - \rho_{ce}}{\rho_{ct}} \tag{2}$$

where, ρ_t and ρ_e are theoretical density and experimental density of the composite samples.

Characterization - Measurement of hardness

Specimens for all composite series were constructed using standard dimensions. A Shore D durometer was used to assess the Shore hardness of GF/PPS/CNF hybrid nanocomposites in compliance with ASTM D2240 [28]. To ensure reproducibility, five measurements were made on each sample at various points. Five samples per composition were examined for each mechanical characterization, and the findings were presented as average values with matching standard deviations. Following stabilization, ten replicates of each composition's hardness measurements were averaged, and the mean ± standard deviation data were utilized for analysis.

Characterization - Short-beam test

The short-beam shear test was used to measure the interlaminar shear strength (ILSS) of the PPS-based hybrid nanocomposites in compliance with ASTM D2344M-22 [29]. The samples were manufactured with a width-to-thickness ratio of 2:1 and a span-to-depth ratio of 6:1. A universal testing machine (UTM-Kalpak Instruments & Controls, India) was used to conduct testing in a three-point bending configuration at 23°C. Up until the sample failed, the crosshead speed remained constant at 1 mm/min. For every formulation, three duplicates were assessed to guarantee statistical reliability. Results are presented as mean ± standard deviation, and strong experimental repeatability is shown by coefficients of variation that are consistently less than 4.6%. The following standard relationship was used to calculate the ILSS:

$$ILSS\left(MPa\right)=\frac{0.75\times P_{max}}{b\times t} \tag{3}$$

where, P_{max} refer to maximum load at failure in N, b stands for width in mm, and t refers to sample thickness in mm.

Characterization - Methodology and experimental design

The Design of Experiments (DoE) proposed by Taguchi was put into practice. Optimizing quality characteristics across many combinations of input factors is a common application of this robust statistical methodology [30]. The experimental runs and subsequent statistical analysis in this study were carried out using Minitab 19 software. An L27 orthogonal array was used to examine five variables at three levels based on the control parameters listed in Tab. 5. Signal-to-Noise (S/N) ratio analysis, which generally divides quality loss functions into nominal-the-best, larger-the-better, or smaller-the-better categories, was used to assess the system's response efficacy. The "smaller-the-better" function was used to find the best wear-rate and friction coefficient, enabling the identification of parameters that result in the least amount of material loss as well as reduced coefficient of friction.

Factor	Unit	Designation	Level		
			I	II	III
Applied Load	N	L	5	10	15
Velocity	m/s	V	0.3	0.4	0.5
Abrading distance	m	D	25	50	75
SiC emery paper	µm	E	36	53	78
Filler	wt%	F	0	0.4	0.8

Table 5: Factor and Levels for 2 BAW Tests

Characterization - Two-body abrasive wear test

PPS-based hybrid nanocomposites' wear and friction characteristics were assessed utilizing a pin-on-disc tribometer with SiC emery paper serving as the abrasive counterface. Fig. 5 shows a schematic of the 2 BAW arrangement. To replicate abrasive conditions, SiC abrasive sheets with particle sizes of 36, 53, and 75 µm were placed on a revolving steel disk. Under the same circumstances, three composite series (C0, C1, and C2) were tested.

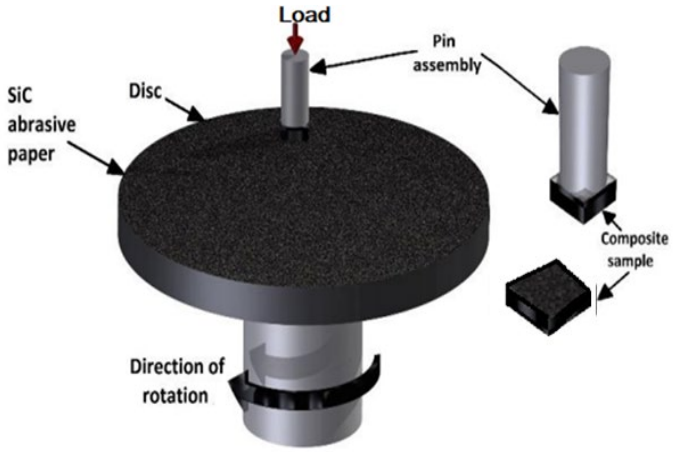

Figure 5: Graphical representation of 2 BAW testing as per ASTM G99.

Wear tests were carried out in compliance with ASTM G99 guidelines at room temperature [31]. Aluminum pins measuring 8 mm in diameter and 30 mm in length were attached to square samples measuring 8 mm × 8 mm × 3.2 mm.

The samples were examined at sliding velocities of 0.3–0.5 m/s with a track diameter of 55 mm. To ensure consistent contact conditions, specimen surfaces were polished using 1200-grit abrasive paper before testing. Fresh abrasive paper was used for each test, and acetone was used to clean the specimens both before and after testing. An electronic balance with a precision of 0.1 mg was used to quantify wear loss; the given data are the mean of three separate experiments.

Characterization - Scanning electron microscopy

Field Emission Scanning Electron Microscopy (FESEM; ZEISS SIGMA) was used to study the worn surface shape and wear mechanisms of the produced hybrid nanocomposites and abrasive emery media. Before analysis, samples underwent an ultrathin gold sputter-coating procedure to reduce surface charging and improve picture resolution. To give a thorough assessment of topographical characteristics and elemental contrast, micrographs were taken in both secondary electron and backscattered electron modes. A strong correlation between the surface damage features and the experimental tribological data was made possible by this dual-imaging approach, which made it easier to precisely determine particle distribution, grain size, and particular wear signatures, such as micro-ploughing, delamination, or debris accumulation [32].

RESULTS AND DISCUSSION

Fourier Transform Infrared Spectroscopy Analysis

Fig. 6 shows the FTIR spectra of neat PPS, GF, and the resulting hybrid nanocomposites (C0, C1, and C2), which show the materials' structural integrity and chemical footprint. The C=C stretching vibrations of the aromatic ring and the C–S stretching mode, respectively, were represented by distinctive peaks in the PPS at 1480.92 cm^{-1} and 1009.95 cm^{-1}. The GF spectra displayed a noticeable absorption band at approximately 888.88 cm^{-1}, which is linked to Si–OH groups and Si–O–Si symmetric stretching vibrations, as seen in Fig. 6. The GFs' surface functionality and chemical structure are responsible for the stability seen in the GF spectrum at the end of the test. The glass fiber surface's natural chemical stability and heat resistance are enhanced by these silicate-based functional groups. Previous investigations have also demonstrated similar stability of glass fiber reinforced polymer composites because of the chemically inert Si–O–Si network [33].

The persistence of PPS-specific peaks in the hybrid nanocomposites (C0, C1, and C2) attests to the thermoplastic matrix's ability to retain its chemical structure after GF and CNFs are added. Significantly, the C1 (0.4 wt% CNF) and C2 (0.8 wt% CNF) samples showed a shift in the aromatic C=C band to 1467.66 cm^{-1} and a faint peak at 2978.44 cm^{-1}, which was attributable to the C–H stretching of the CNF backbone. This little shift indicates the existence of pi-pi interactions between the graphitic structure of the CNFs and the aromatic rings of the PPS matrix. Additionally, the nanocomposites' distinctive peak at 805.14 cm^{-1} shows the para-substituted benzene rings' out-of-plane C–H bending, which is more pronounced in the modified samples. These results are consistent with recent research indicating that adding carbonaceous nanofillers to semi-crystalline polymers like PPS may cause local molecular rearrangements that could improve interfacial adhesion [33, 34]. The absence of notable new peaks suggests that PPS reinforcement with CNFs is mostly a physical interaction rather than a covalent chemical alteration, maintaining the matrix's intrinsic thermal stability.

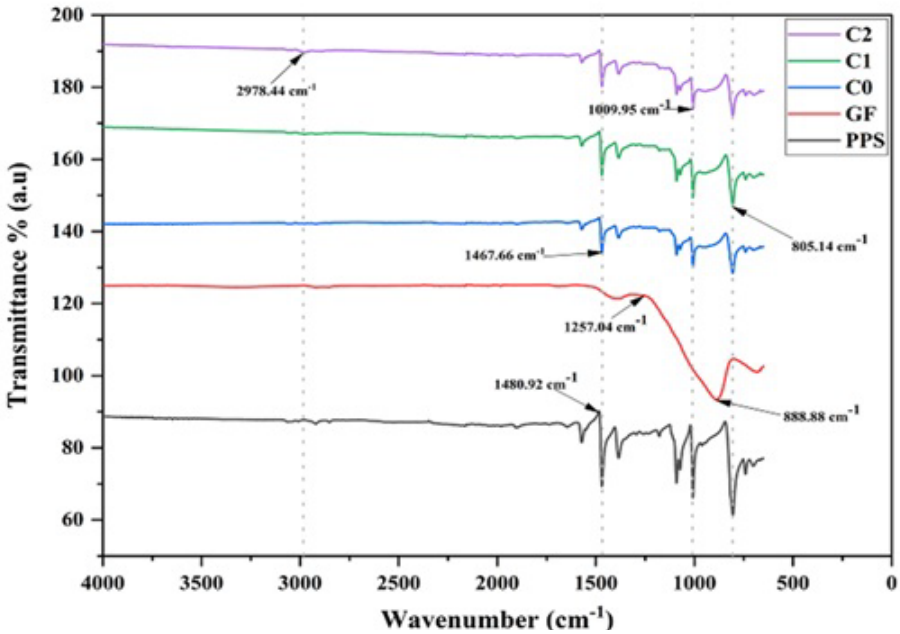

Figure 6: FTIR Spectroscopic analysis of CNF modified GF/PPS hybrid nanocomposites.

Density, Voids, Hardness, and Interlaminar Shear Strength of GF/PPS/CNF hybrid nanocomposites

In comparison to the baseline composite (unfilled C0), the density, void content, hardness, and interlaminar shear strength (ILSS) of PPS/GF/CNF hybrid composites clearly depend on CNF content as listed in Tab. 6. Because E-glass fibers (2.54 g/cm³) and CNFs (2.1 g/cm³) have greater intrinsic densities than PPS (1.35 g/cm³), the experimental density increased from 1.619 g/cm³ (C0) to 1.625 g/cm³ (C1) and 1.659 g/cm³ (C2). The void content decreased in C2 (0.48%), suggesting better packing and interfacial bonding with higher CNF loading, but slightly increased in C1 (0.79%) due to potential agglomeration at lower CNF dispersion.

Composite (Codes)	Density (g/cm³)	Density (g/cm³)	% Voids	Hardness (Shore D)	% increase	ILSS (MPa)	% increase
C0	1.624	1.619 ± 0.2	0.31	77.5 ± 0.8	---	28.7 ±1.3	---
C1	1.638	1.625 ± 0.2	0.79	87.02 ± 0.5	12.28	31.3 ±1.1	9.06
C2	1.667	1.659 ± 0.2	0.48	93.03 ± 0.9	20.04	35.5 ±1.2	23.69

Supplier's data: Density of E-GF 2.54 g/cm³, Density of CNF 2.1 g/cm³, Density of PPS 1.35 g/cm³

Table 6: Density and voids of fabricated PPS/GF/CNF hybrid nanocomposites.

The stiffening effect and homogeneous stress distribution given by high aspect ratio CNFs are responsible for the significant improvement in hardness from 77.5 (C0) to 87.02 (C1) and 93.03 (C2), with a maximum increase of almost 20%. Like this, ILSS increased from 28.7 MPa (C0) to 35.5 MPa (C2), demonstrating a 23.7% improvement as a result of enhanced crack-bridging and fiber-matrix interfacial adhesion mechanisms. The PPS/GF/CNF hybrid nanocomposites observed increases in density, decreased void content, hardness, and ILSS are in line with research findings published in the literature. Through better load transmission and molecular-level interactions, the addition of carbon-based nanofillers like graphene and CNTs improves mechanical and tribological properties, according to studies like Y. Li et al. [35]. Similarly, using predictive modeling techniques, Demir et al. [36] showed that nano filler filled GF composites perform better mechanically and tribologically because of improved dispersion and fewer voids. Additionally, improvements in the mechanical and electrical properties of polymer composites reinforced with CNFs were reported by Li et al. [37], who attributed these improvements to better filler network development and interfacial bonding. The current results, which demonstrate increased hardness (20%) and ILSS (23.7%) when compared to these studies, validate the efficacy of hybrid nanofiller reinforcement in high-performance polymer composites by confirming that the addition of CNFs significantly strengthens fiber/matrix adhesion, minimizes microvoids, and promotes efficient stress transfer.

Two-body abrasive wear of CNF modified GF/PPS composites

The design of experiments (DoE) technique, which is successfully applied through the Taguchi method utilizing an L27 orthogonal array generated by the Minitab 19 program with five parameters of three levels each, is used to conduct 2 BAW tests. Tab. 7 displays the signal-to-noise ratios (S/N R) derived from the program for the wear loss and coefficient of friction findings obtained from experimentation.

The wear loss and CoF of GF/PPS composites are significantly impacted by the addition of CNF (Tab. 7). In comparison to C0, composites containing 0.4 wt% (C1) and 0.8 wt% (C2) CNFs show a noticeable decrease in wear loss, suggesting improved tribological performance. This enhancement is explained by CNFs' capacity to increase load-bearing capacity and function as solid lubricants, which lessens material removal and asperity interaction. CoF therefore drops as CNF content rises, with C2 exhibiting the lowest values because of the creation of a stable transfer film and smoother sliding behavior.

Similar patterns were noted by Li et al. [35], who emphasized improved load transfer and interfacial interactions with carbon-based nanofillers and Demir et al. [36], who focused on increased dispersion and fiber–matrix bonding. At the ideal 0.8 wt% loading, improved adhesion in C1 and C2 prevents fiber pull-out, matrix cracking, and delamination, allowing for effective stress transfer. Agglomeration and decreased performance, however, could result from using too much filler.

The experimental wear loss and coefficient of friction data, as well as the related S/N ratios, were used to revalidate the optimization results (Tab. 7). The multi-response optimization behavior, in which minimal wear loss and minimum coefficient of friction do not always occur at identical parameter combinations, is responsible for variations seen under specific conditions. Thus, based on the combined effects of load, sliding velocity, abrading distance, SiC grit size, and filler content, the chosen ideal circumstances represent the highest overall tribological performance.

The reinforcing effectiveness of CNFs, which improves hardness, stiffness, and mechanical integrity by creating a strong network that resists deformation and material loss, is largely responsible for the improved wear resistance and decreased CoF. Siengchin reported similar gains [38]. Furthermore, CNFs reduce shear stress and stabilize friction by acting as a protective barrier and encouraging the production of transfer films [39]. In addition to reducing deformation and frictional heating [40], their natural lubricating properties and enhanced dispersion further increase interfacial adhesion and wear resistance [41]. According to Praveena [42], shore D hardness and low-velocity impact energy increased, demonstrating enhanced toughness through fiber-assisted crack bridging and arrest and superior resistance to surface

indentation. In summary, homogeneous dispersion and improved tribological performance are ensured by optimal CNF loading; in line with earlier research, C2 (0.8 wt%) shows the best wear resistance and lowest CoF.

Run	Load (N)	SV (m/s)	AD (m)	SiC Paper (µm)	Filler (wt%)	Wear loss (g)	SNR For Wear loss	CoF	S/N R for CoF
1	5	0.3	25	36	0	0.0063	44.0132	0.338	9.4217
2	5	0.4	50	53	0.4	0.0106	37.6523	0.332	9.9039
3	5	0.5	75	78	0.8	0.0436	27.2103	0.328	9.6825
4	10	0.3	50	78	0.4	0.0184	34.7510	0.316	9.9515
5	10	0.4	25	36	0.8	0.0127	37.9239	0.321	9.8699
6	10	0.5	75	53	0	0.0309	30.1448	0.324	9.8429
7	15	0.3	75	53	0.8	0.0119	38.4891	0.299	10.4866
8	15	0.4	50	36	0	0.0178	34.9916	0.307	10.2572
9	15	0.5	25	78	0.4	0.0353	29.0445	0.301	10.4287
10	5	0.3	75	78	0	0.0111	39.0935	0.318	9.9515
11	5	0.4	50	53	0.4	0.0152	36.6231	0.307	10.0118
12	5	0.5	25	36	0.8	0.0182	34.7986	0.305	10.3140
13	10	0.3	25	53	0.4	0.0106	39.4939	0.341	9.3449
14	10	0.4	75	78	0.8	0.0349	29.1435	0.324	9.7891
15	10	0.5	50	36	0	0.0226	32.9178	0.361	8.8499
16	15	0.3	50	36	0.8	0.0085	41.4116	0.262	11.6340
17	15	0.4	25	78	0	0.0361	28.8499	0.281	11.0259
18	15	0.5	75	53	0.4	0.0412	27.7021	0.271	11.3406
19	5	0.3	50	78	0.8	0.0091	40.6303	0.327	9.6825
20	5	0.4	75	53	0	0.0154	36.2496	0.347	9.1934
21	5	0.5	25	36	0.4	0.0122	38.2728	0.334	9.5251
22	10	0.3	75	36	0.4	0.0083	41.6184	0.328	9.6825
23	10	0.4	50	78	0.8	0.0601	24.4225	0.322	9.8429
24	10	0.5	25	53	0	0.0249	32.1110	0.333	9.6034
25	15	0.3	25	78	0.4	0.0252	31.9720	0.283	10.9643
26	15	0.4	75	36	0.8	0.0152	36.3631	0.273	11.2767
27	15	0.5	50	53	0	0.0362	28.8258	0.295	10.6036

Table 7: Wear loss, CoF and SNR of GF/PPS/CNF hybrid nanocomposites.

Main effect plots for wear loss

The primary impacts of load, abrading distance (AD), sliding velocity (SV), filler content, and SiC paper particle size on wear loss are shown in Fig. 7. Higher contact stress and frictional heating speed up material removal, as seen by a growing trend in wear loss with increasing load and sliding velocity. Similarly, extended exposure to abrasive interaction causes wear loss to modestly increase with abrading distance.

Archard's wear law, hardness, and interlaminar shear strength (ILSS) can all be succinctly correlated with the observed tribological behavior. The improvement in the composite's hardness and ILSS is closely linked to the decrease in wear loss under optimal CNF loading (0.8 wt%). Higher hardness limits the penetration of abrasive SiC particles by improving the material's resistance to plastic deformation and microcutting. Higher ILSS also indicates better fiber–matrix interfacial bonding, which inhibits surface delamination and fiber pull-out during abrasion. This reduces material loss by creating a more stable surface and encouraging the development of a protective tribo-film. In line with Archard's law, wear volume is inversely related to hardness but directly correlated with load and sliding distance. Therefore, the observed decrease in wear loss can be directly explained by the increase in hardness with the addition of CNF. Furthermore, by reducing debris production and crack propagation, stronger interfacial adhesion successfully reduces the wear coefficient.

This framework is further supported by the impact of SiC particle size and SV: finer abrasives improve real contact area and cutting efficiency, increasing wear despite material strengthening, while greater SV increases interaction frequency, intensifying material removal. While abrasive size and SV continue to be the primary external governing factors, the

synergistic improvement in hardness and ILSS at optimal CNF concentration improves load-bearing capacity and structural integrity, consequently lowering wear in accordance with Archard's principle.

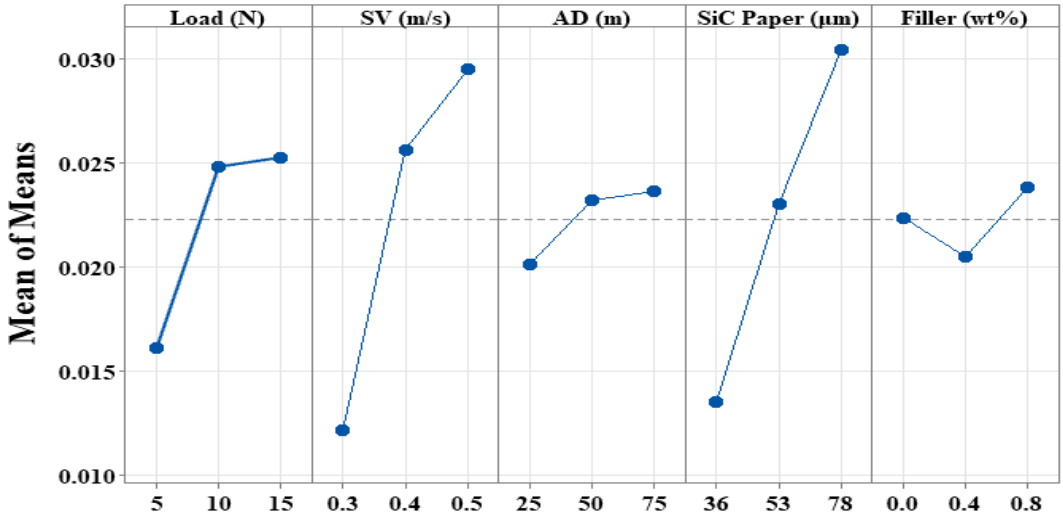

Figure 7: Main effect plots for wear loss.

Interaction plots for wear loss

The interaction effects of process parameters on wear loss are shown in Fig. 8, emphasizing the combined impact of operating conditions. There is a significant connection between load and SV, with wear loss increasing more sharply at higher loads and higher velocities because of increased surface damage and frictional heating. Similarly, wear is much higher at higher loads with finer abrasives, demonstrating severe micro-cutting and ploughing mechanisms, according to the interplay between load and SiC particle size.

Higher velocities and higher SiC particle sizes result in the greatest wear loss, demonstrating the significant interaction between SV and SiC particle sizes that was found in the ANOVA. On the other hand, interactions involving abrading distance (AD) are rather modest, exhibiting merely a slow rise in wear with increasing distance independent of other variables.

There is a discernible relationship between filler content and load and SV, with optimal filler loading (about 0.8 wt%) consistently leading to reduced wear under various circumstances. But compared to SV and SiC particle size, the effect is less sensitive, indicating that CNFs mainly increase wear resistance by stabilizing the surface rather than drastically changing the interaction trends.

Overall, the plots show that wear loss is very sensitive to the combined impacts of SiC particle size, SV, and load, while CNF incorporation reduces wear in all scenarios, with appropriate filler loading showing the best results.

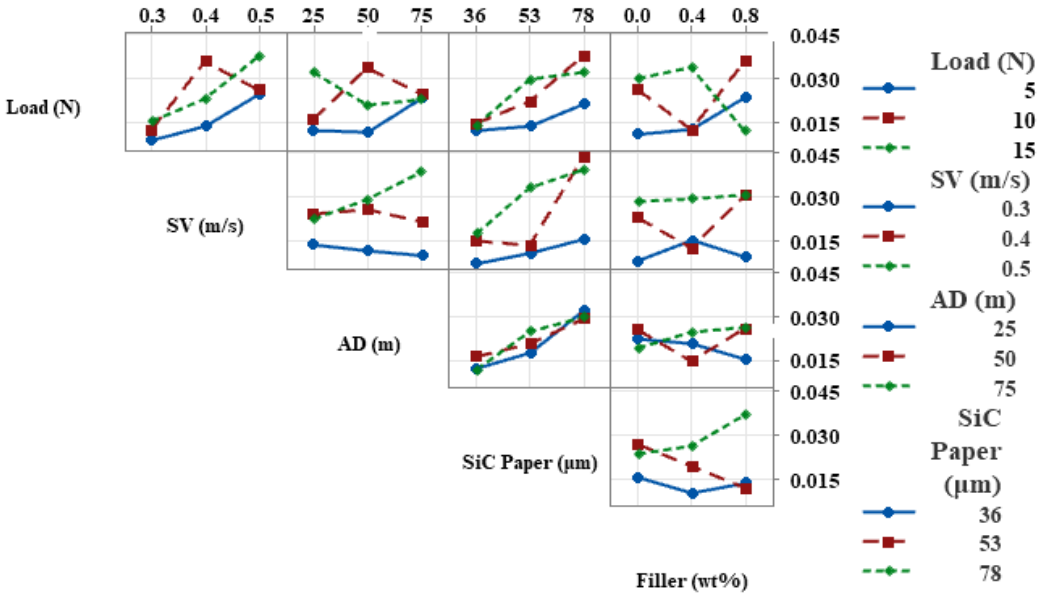

Figure 8: Interaction plots for wear loss.

ANOVA for wear loss

Tab. 8 displays the ANOVA results assessing the statistical relevance of process parameters on wear loss. A higher F-value denotes a greater influence on the response variable since it shows the ratio of the variation explained by each factor to the unexplained experimental error. A significant effect at a 95% confidence level is indicated by a p-value of less than 0.05.

Sliding velocity (SV) and SiC abrasive particle size had the greatest F-values (13.40 and 12.40, respectively) and very low p-values (≤ 0.001) among the examined parameters, indicating that they are the most statistically significant factors controlling wear loss. This suggests that material removal methods are dominated by both abrasive severity, which is regulated by SiC particle size, and frictional heating effects, which are linked to SV. Although its relative contribution is smaller than that of SV and SiC particle size, load also has a statistically significant impact on wear loss ($F = 3.95$, $p = 0.040 < 0.05$). Conversely, axial distance (AD) ($F = 0.23$, $p = 0.797$) and filler content ($F = 0.30$, $p = 0.747$) show strong p-values (> 0.05), suggesting that their effects are statistically negligible within the examined range.

Good experimental reproducibility is indicated by the error term remaining small. Additionally, the lack-of-fit is statistically non-significant ($p = 0.299 > 0.05$), indicating that the generated model accurately and significantly depicts the experimental data. As a whole, the findings show that sliding velocity and SiC particle size are the main factors influencing wear loss, followed by load; under the conditions under investigation, AD and filler content have very little statistical impact.

.Source	DF	Adj SS	Adj MS	F-Value	P-Value
Load (N)	2	0.000517	0.000259	3.95	0.040
SV (m/s)	2	0.001756	0.000878	13.40	0.000
AD (m)	2	0.000030	0.000015	0.23	0.797
SiC Paper (μm)	2	0.001624	0.000812	12.40	0.001
Filler (wt%)	2	0.000039	0.000019	0.30	0.747
Error	16	0.001048	0.000065		
Lack-of-Fit	15	0.001037	0.000069	6.54	0.299
Pure Error	1	0.000011	0.000011		
Total	26	0.004755			

Table 8: ANOVA results for main effect on wear loss

Regression equation and residual plots for wear loss

The association between wear loss and the input parameters is established by the created quadratic regression model (Eqn. 1), suggesting that wear is positively influenced by all factors. According to the coefficients, sliding velocity (SV) has the biggest impact (0.1022), followed by SiC paper grit and filler content. The impacts of load and abrading distance (AD) are comparatively smaller. This suggests that whereas AD has no effect, an increase in SV greatly speeds up wear because of increased frictional energy and thermal effects.

$$Wear\ loss\left(g\right) = -0.0575 + 0.00095\,Load\left(N\right) + 0.1022\,SV\left(\frac{m}{s}\right) + 0.000052\,AD\left(m\right) + \\ + 0.00045\,SiC\ paper\left(\mu m\right) + 0.00364\,Filler\left(wt\%\right) \tag{4}$$

The model has a fair predictive capability, as evidenced by the coefficient of determination ($R^2 = 73.49\%$), which shows that it explains a significant amount of the variability in wear loss. The model is statistically appropriate without undue overfitting, as confirmed by the somewhat lower but still acceptable adjusted R^2 (67.18%), which takes into consideration the number of predictors.

The residual diagnostics used to validate the regression model are displayed in Fig. 9. The normality of the residuals is confirmed by the normal probability plot, which shows a near-linear trend. Random scatter is seen in the residuals vs. fitted values, showing no systematic error and constant variance. In a similar vein, there is no trend in the residuals vs. observation order, indicating independence. For estimating wear loss, the model is often dependable and statistically sufficient.

Main effect plots for coefficient of friction

The main effects of process variables on the coefficient of friction (CoF) are shown in Fig. 10. With increasing load, a significant declining trend is seen, suggesting better surface conformance and less interfacial shear at higher loads. Sliding velocity only slightly varies, and at higher velocities, CoF somewhat increases, probably because of frictional heating effects. With slight variations in CoF, AD shows a weak, non-linear contribution, indicating a limited impact within the examined range. In a similar vein, SiC particle size exhibits a small effect, with finer abrasives modestly increasing CoF because of increased asperity interaction.

On the other hand, filler content shows a distinct and steady decrease in CoF, with values gradually declining up to 0.8 wt%, demonstrating the efficient lubricating function of CNFs through stable transfer film development. Overall, SV, AD, and SiC particle size have relatively small influence on CoF, whereas load and filler content are the main variables.

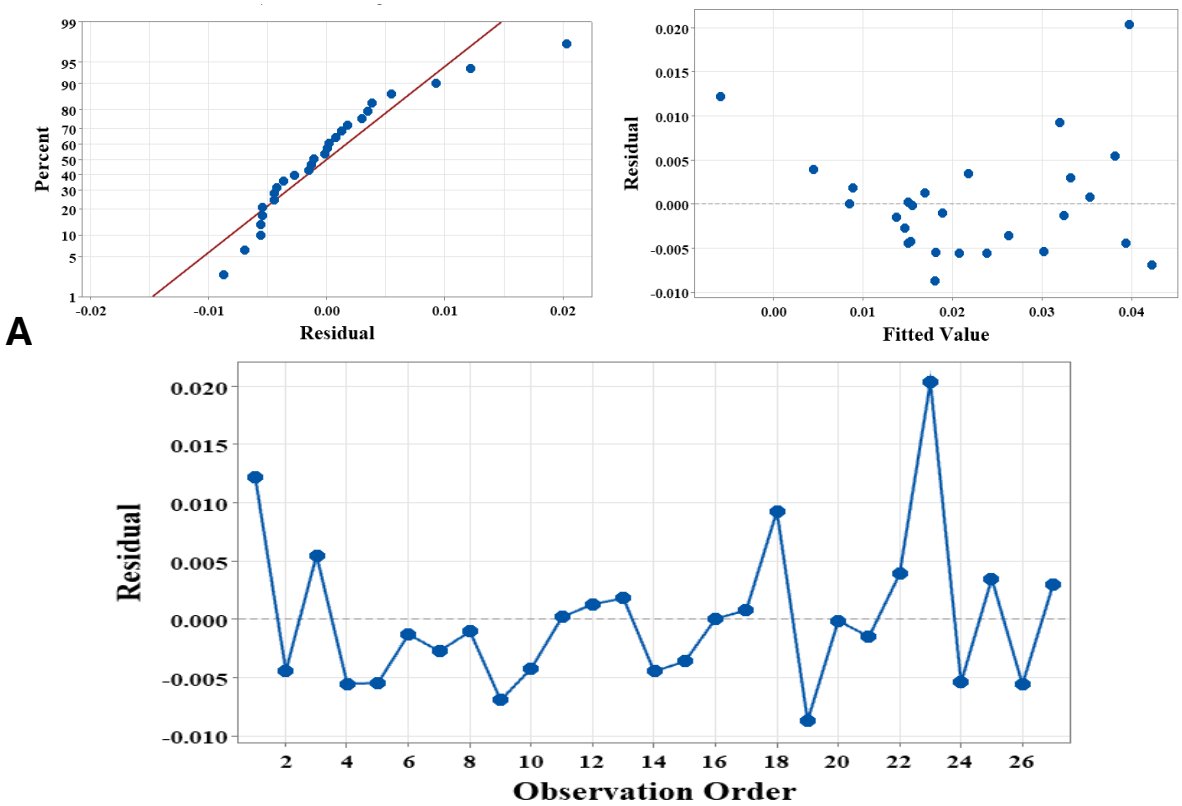

Figure 9: Residual plots for wear loss model.

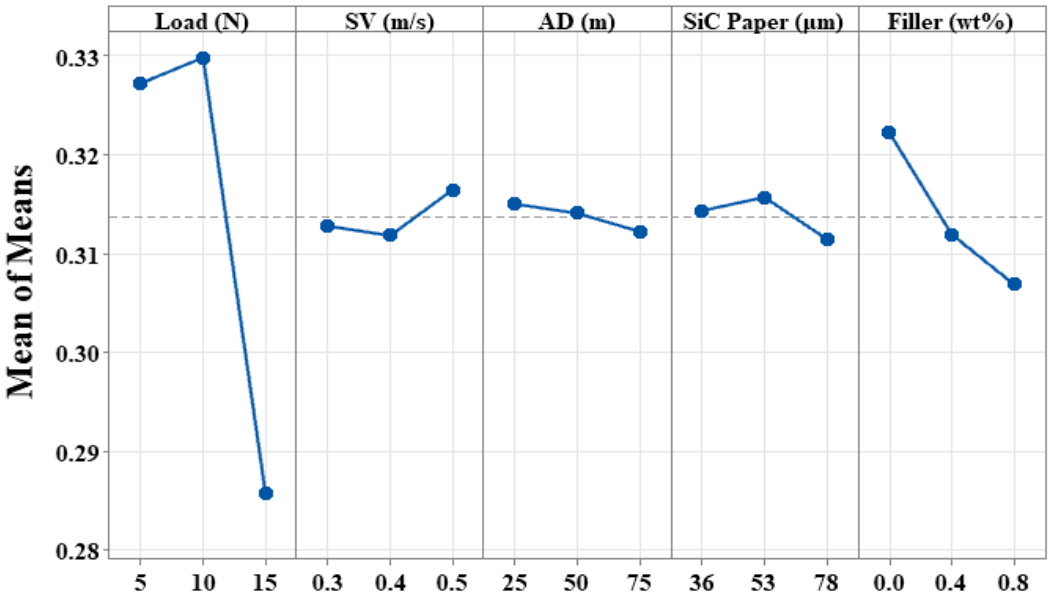

Figure 10: Main effect plots for coefficient of friction.

Interaction Plots for coefficient of friction

The interaction effects of process parameters on CoF are depicted in Fig. 11, emphasizing the combined impact of operating circumstances. There is a discernible interaction between load and SV, where CoF lowers with increased load because of better surface conformity and less shear resistance, but it slightly increases with increasing SV, perhaps because of frictional heating.

Owing to the load–SiC interaction, larger loads coupled with coarser particle size lower friction, while finer abrasives often yield higher CoF due to enhanced asperity contact. In a similar vein, the SV and SiC interaction exhibits increased CoF with finer abrasives at higher velocities. Abrading distance (AD) interactions are rather weak, exhibiting only slight

changes in CoF. Filler content, on the other hand, consistently reduces friction under most circumstances, with 0.4–0.8 wt% CNFs encouraging sustained transfer film development. While SV and abrasive particle size show associated secondary effects, load and filler content generally dominate CoF reduction.

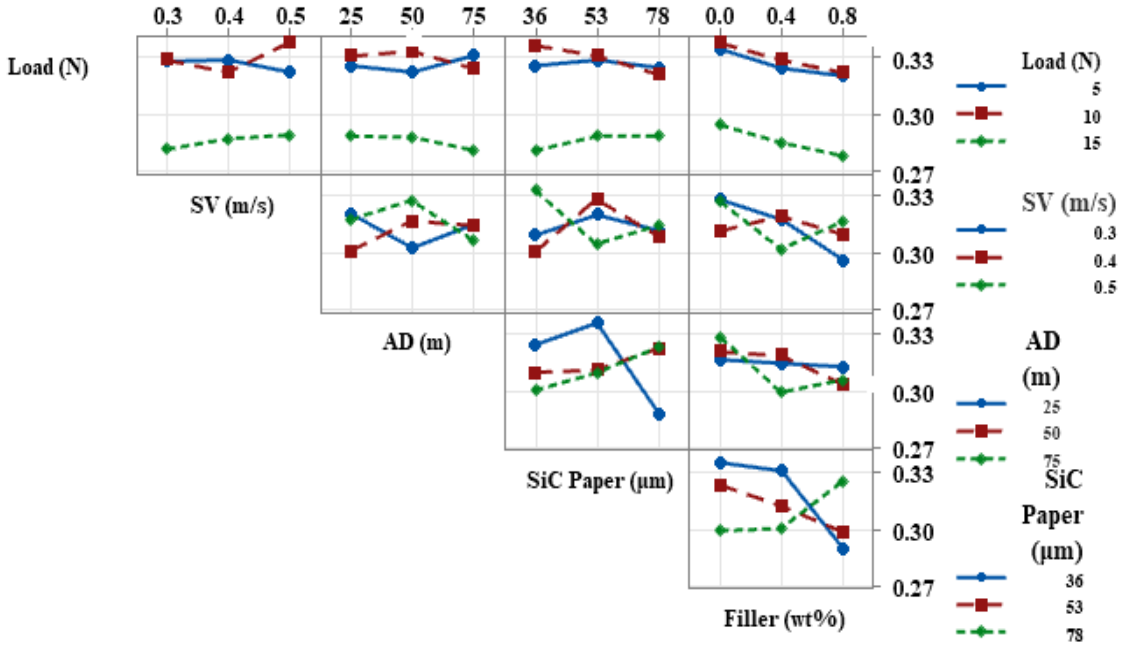

Figure 11: Interaction plots for coefficient of friction.

ANOVA for coefficient of friction

The ANOVA results Tab. 9 show that load is the only statistically significant factor affecting CoF ($F = 22.48$, $P = 0.008 < 0.05$), indicating its primary participation in frictional behavior. On the other hand, strong P-values (> 0.05) for SV, AD, SiC particle size, and filler content indicate statistically insignificant individual impacts within the examined range. Filler has a larger contribution among these, but it is still not significant. The constructed model's adequacy is confirmed by the non-significant lack-of-fit ($P = 0.733$). Overall, load is the main factor influencing CoF; other factors either have a minor impact or do so through interaction effects.

Source	DF	Adj SS	Adj MS	F-Value	P-Value
Load (N)	2	0.010778	0.005389	22.48	0.008
SV (m/s)	2	0.000011	0.000005	0.02	0.978
AD (m)	2	0.000016	0.000008	0.03	0.968
SiC Paper (µm)	2	0.000011	0.000006	0.02	0.977
Filler (wt%)	2	0.000911	0.000455	1.90	0.182
Error	16	0.003836	0.000240		
Lack-of-Fit	15	0.003524	0.000235	0.75	0.733
Pure Error	1	0.000313	0.000313		
Total	26	0.015731			

Table 9: ANOVA results for main effect on coefficient of friction.

Regression equation and residual plots for coefficient of friction

The regression Eqn. (5) establishes the quantitative relationship between CoF and the governing parameters, highlighting both the direction and relative influence of each factor. The negative coefficients for load (−0.004056), sliding velocity (−0.0045), abrading distance (−0.000018), and filler content (−0.00187) indicate a reduction in CoF with increasing parameter levels. Among these, sliding velocity and load exert the most pronounced influence, suggesting that higher contact severity facilitates stable tribolayer formation and reduces interfacial shear. The negative coefficient of filler confirms the lubricating role of CNFs through transfer film development.

$$CoF(\mu) = 0.3635 - 0.004056\,Load(N) - 0.0045\,SV\left(\frac{m}{s}\right) - 0.000018\,AD(m) + \\ + 0.000042\,SiC\ Paper(\mu m) - 0.00187\,Filler(wt\%) \tag{5}$$

Conversely, SiC particle size exhibits a positive coefficient (+0.000042), implying a slight increase in CoF due to enhanced asperity interaction. The intercept (0.3635) represents the baseline CoF. Overall, load and SV dominate friction reduction, while other factors show comparatively minor effects.

The coefficient of friction linear regression model has an R^2 of 0.7734, which means that the model explains 77.34% of the total variability. After taking the number of predictors into consideration, the modified R^2 of 69.25% shows a modest level of predictive reliability. However, the relatively small, adjusted value and the difference between R^2 and adjusted R^2 indicate that the linear model may not adequately represent the intricacy of the CoF response. This suggests that there are important interaction effects and non-linear interactions between the process parameters, which the current linear formulation does not sufficiently capture.

The residuals are roughly normally distributed, as seen in Fig. 12, where most of the dots follow the reference line. The random dispersion about zero in the residuals vs. fitted figure suggests constant variance and no discernible model bias. The absence of a systematic trend in the residuals vs. observation order confirms the independence of mistakes. The model's underlying assumptions are largely met.

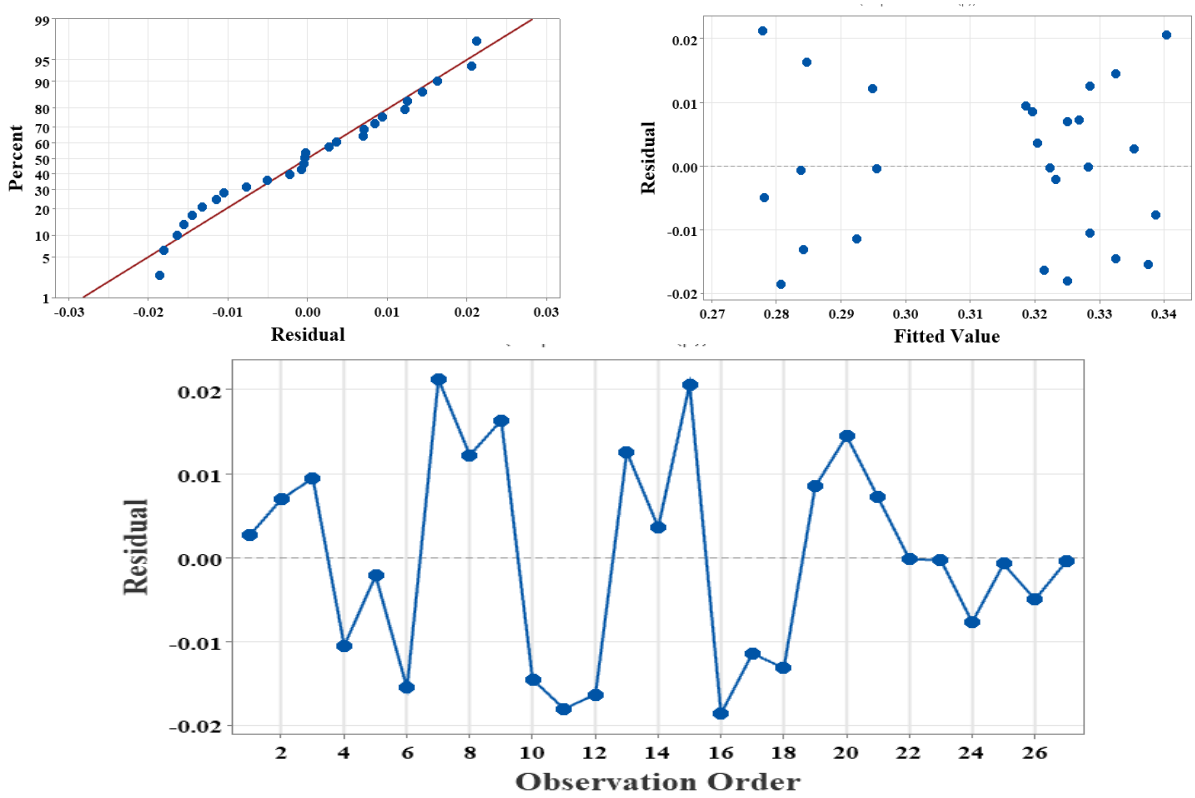

Figure 12: Residual plots for coefficient of friction model.

Confirmation test for wear loss and coefficient of friction

For both wear loss and coefficient of friction (CoF) of GF/PPS/CNF hybrid nanocomposites, the confirmation test findings shown in Tab. 10 show a strong agreement between the experimental values and the regression model predictions. Systematic adjustment of SiC particle size and filler content produced consistent trends under constant testing settings (8 N load, 0.45 m/s sliding velocity, and 40 m abrading distance), which the created models accurately reflected. Whereas CoF prediction errors fell between 2.86% and 6.50%, wear loss percentage errors varied between 3.73% and 5.09%. Interestingly, Trial 3 showed the best prediction accuracy with the lowest wear loss deviation (3.73%). The robustness and dependability of the regression models for forecasting tribological performance are generally confirmed by the low error margins (all below ~6.5%).

Trails	Experiment wear loss (g)	Regression model Wear loss (g)	% Error	Experiment CoF	Regression model CoF	% Error
1	0.0157	0.0149	5.09	0.3538	0.3308	6.50
2	0.0223	0.0234	4.93	0.3321	0.3226	2.86
3	0.0375	0.0361	3.73	0.3273	0.3141	4.03

Table 10: Confirmation test results for wear loss and CoF.

Contour plots for wear loss

The contour plots shown in Figs. 13(a–d) are in good agreement with the ANOVA results (Tab. 8) and offer a clear graphical depiction of the combined impact of process factors on wear loss. The figures clearly reveal that the two most important elements affecting wear behavior are sliding velocity (SV) and the size of SiC abrasive paper, whilst load has a moderate effect and abrading distance (AD) and filler content have a relatively weaker influence within the examined range.

The interaction between filler content and load in Fig. 13(a) shows that at moderate load levels, wear loss stays in the low regime (dark blue region, < 0.01 g); nevertheless, an increase in load above 10 N gradually moves the response toward greater wear zones. This pattern supports the load's statistical significance as shown by ANOVA. Filler content against SV in Fig. 13(b) makes it evident that wear loss increases dramatically with SV beyond about 0.40–0.45 m/s, moving from low-wear to higher-wear regions. This provides strong evidence that SV is the most relevant parameter, as indicated by its greatest F-value.

In line with its high p-value and low F-value in ANOVA, Fig. 13(c) (filler vs. AD) displays a comparatively uniform contour distribution with only minor variance in wear loss over the AD range, suggesting that AD has little impact on wear behavior. Similar to this, Fig. 13(d) (filler vs. SiC paper size) shows a clear shift in wear response as abrasive size increases, with coarser SiC particles resulting in noticeably greater wear loss. This demonstrates that SiC particle size is the second most important element influencing material removal and abrasive severity.

At moderate filler concentration (~0.3–0.5 wt%), a localized minimal wear region is seen throughout all contour plots, indicating a minor reinforcing and debris-stabilizing action at optimal loading. Saturation or agglomeration effects of the filler are indicated by the lack of improvement beyond this range. Overall, the contour maps show the ideal operating window for reducing wear loss in the created hybrid composites, confirm the regression model, and offer a clear visual understanding of parameter interactions.

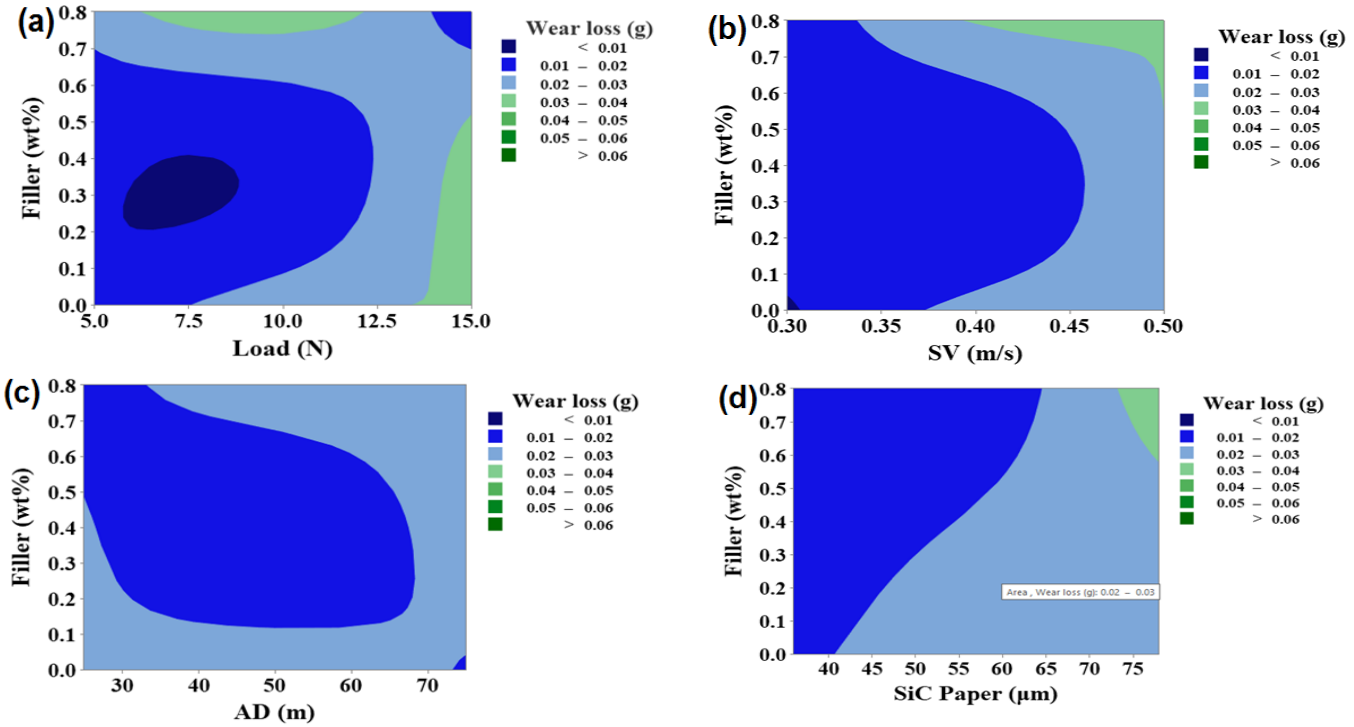

Figure 13: Contour plots for wear loss: (a) Filler (wt%) vs Load (N), (b) Filler (wt%) vs SV (m/s), (c) Filler (wt%) vs AD (m), (d) Filler (wt%) vs SiC Paper (µm).

Contour plots for coefficient of friction

The combined effects of filler content, sliding velocity (SV), abrading distance (AD), load, and SiC abrasive paper size on the coefficient of friction (CoF) are shown by the contour plots in Fig. 14(a–d), which clearly validate the trends found in the ANOVA findings (Tab. 8). Overall, the response surfaces show that the main factors affecting CoF are SV, load, and SiC particle size, with AD having a relatively less impact within the range under study.

The interaction between filler content and SiC paper size in Fig. 14(a) demonstrates a progressive fluctuation in CoF, with larger abrasive size (coarser SiC paper) increasing friction because of increased ploughing and micro-cutting action. Filler has a modest but stabilizing effect on lowering friction fluctuations, as evidenced by the response's relative stability at lower filler contents.

Filler content against AD is plotted in Fig. 14(b), which shows a limited area of greater CoF at intermediate AD values (40–55 m). This suggests that variations in contact length and debris interaction have a moderate impact on frictional behavior. The overall variation is still small, though, indicating that AD has less of an impact than other factors.
It is evident from Fig. 14(c) (filler vs. SV) that CoF rises with sliding velocity, peaking in the mid-range (around 0.35–0.40 m/s) as a result of increased interfacial heating and unstable tribofilm development. A little decrease in CoF is seen at greater filler concentration (~0.3–0.5 wt%), suggesting that the filler has a partial lubricating and load-sharing impact before agglomeration effects take over at higher loading.
Filler content against load is plotted in Fig. 14(d), which shows that CoF increases steadily with increasing load, especially beyond ~10 N, because of increased actual contact area and intensified adhesive interactions. However, by enhancing surface stability and lowering direct asperity contact, filler somewhat mitigates this rise.
Overall, the contour maps support the statistical conclusions that the main causes of frictional behavior are SV and load, followed by SiC particle size, with AD having a negligible impact. Additionally, the plots indicate an ideal filler concentration range (~0.3–0.5 wt%) where enhanced interfacial reinforcement and tribofilm stability result in a balanced decrease in CoF.

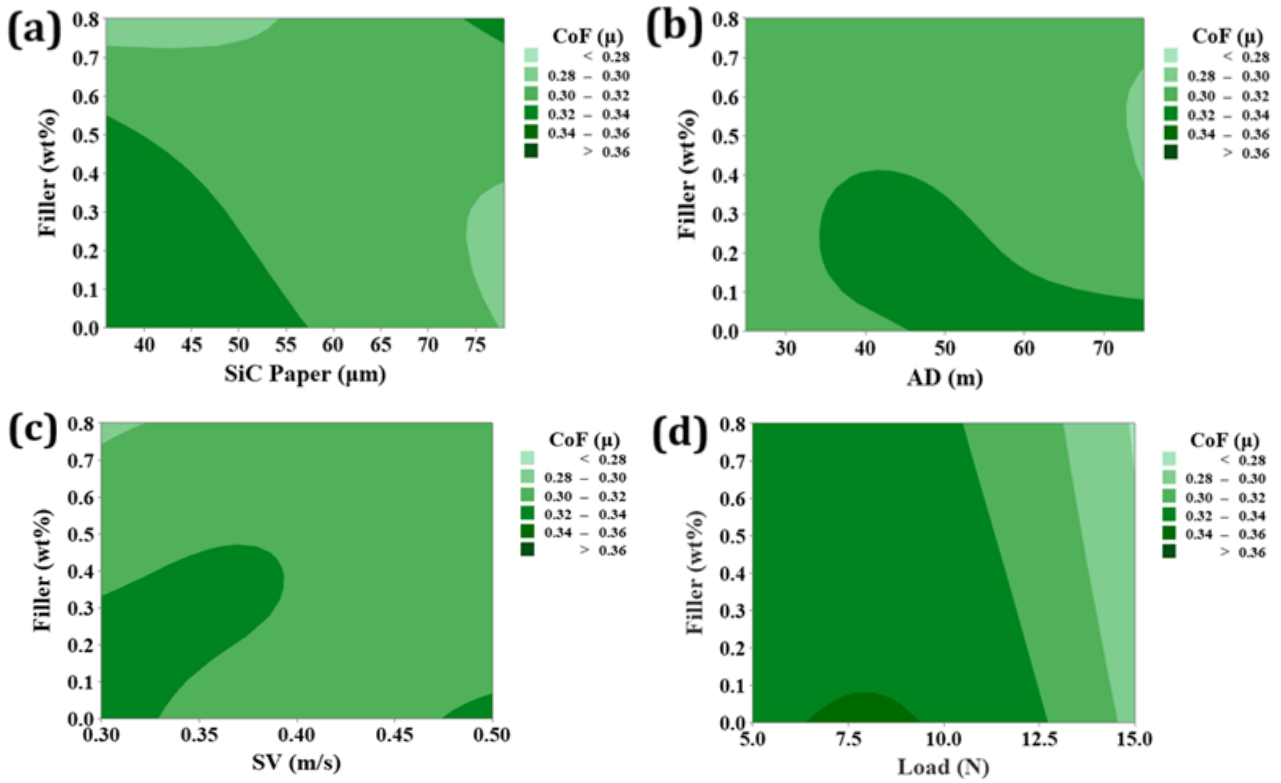

Figure 14: Contour plots for CoF: (a) Filler (wt%) vs Load (N), (b) Filler (wt%) vs SV (m/s), (c) Filler (wt%) vs AD (m), (d) Filler (wt%) vs SiC Paper (µm).

Worn Surface features and wear mechanisms of CNFs modified GF/PPS hybrid nanocomposites

To assess the impact of CNF content on the abrasion resistance and coefficient of friction (CoF) of GF/PPS hybrid nanocomposites, the worn surface morphologies obtained after an abrading distance of 75 m using 78 µm SiC emery paper under a load of 10 N and a sliding velocity of 0.4 m/s were analyzed using SEM. Figs. 15–17 display the corresponding micrographs for C0, C1, and C2, illustrating how surface damage features alter with increasing CNF incorporation.
Figs. 15a and 15b show that the unfilled GF/PPS composite (C0) has significant abrasion degradation on its worn surface. While the higher magnification image (Fig. 15b) clearly displays fiber exposure and pull-out, suggesting weak interfacial adhesion between the GFs and PPS matrix, the low-magnification micrograph (Fig. 15a) shows deep, continuous grooves aligned along the abrading direction, indicating dominant micro-cutting by hard SiC abrasives. Furthermore, repeated abrasive passes and localized thermal softening cause considerable matrix smearing and plastic deformation. By emphasizing the acute abrasive asperities that cause aggressive material removal, Fig. 15c, which displays the SiC emery paper, further demonstrates the intensity of abrasion. Progressive surface deterioration is indicated by the collection of debris and microcracks throughout the worn surface.
These morphological characteristics verify that severe micro-cutting and ploughing, fiber debonding and pull-out, and substantial matrix deformation under repeated loading are the main factors controlling the wear process in C0. Higher wear loss and the inability to form a solid protective tribo-layer are the results of the lack of CNF reinforcement, which

restricts effective load transfer and structural stability. This behavior is in line with observations that have been reported in thermoplastic composites, where material loss and abrasive wear are accelerated by inadequate interfacial bonding [43-45].

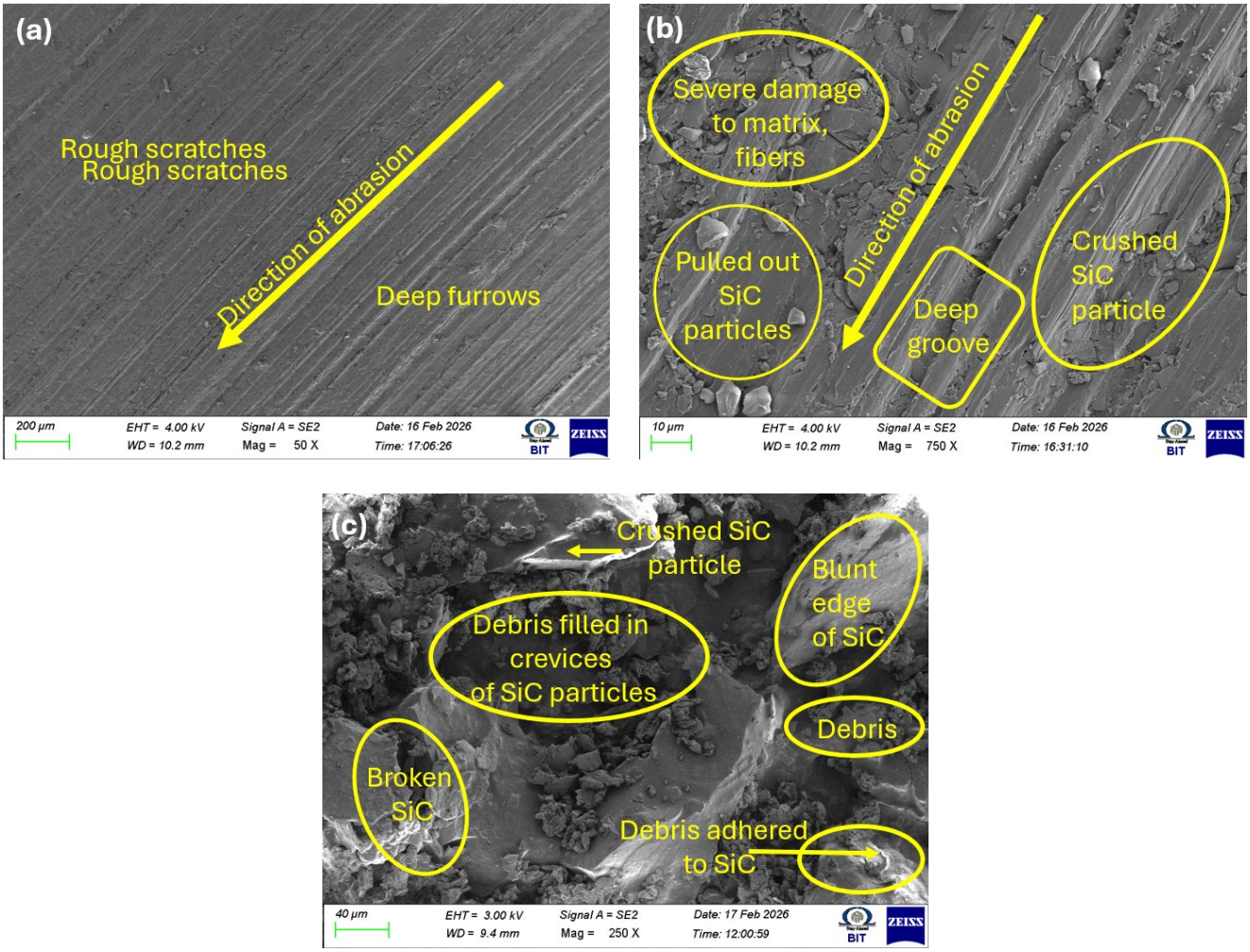

Figure 15: Worn surface micrographs of unfilled GF/PPS composites: (a) 50 X, (b) 250 X, (c) Emery paper used.

As seen in Figs. 16a and 16b, the worn surface morphology of the 0.4 wt% CNF reinforced GF/PPS composite (C1) is comparatively smoother and more uniform than that of the unfilled composite. While the higher magnification micrograph (Fig. 16b) shows noticeably less fiber pull-out, suggesting improved interfacial bonding between the glass fibers and PPS matrix due to the bridging effect of CNFs, the low-magnification image (Fig. 16a) reveals shallower grooves with reduced ploughing depth, indicating improved resistance to abrasive penetration. Furthermore, a thin, irregular tribo-film that partially protects the surface while sliding is shown to form. There are also minor characteristics that show confined stress concentration zones, such as tiny cracks and localized micro-delamination. The shape of the abrasive SiC surface following wear testing is clearly visible in Fig. 16c. The white-bounded areas match the surface of the new SiC abrasive paper, indicating that SiC asperities directly participate in abrasion. Additionally, very small wear particles and thin layers of compacted debris imbedded on the SiC surface are seen, suggesting material transfer and debris adherence during sliding. These attached debris layers prevent severe ploughing action and lessen direct asperity interaction. These findings verify that, with localized debris compaction and surface protection, the wear mechanism eventually shifts from severe abrasive wear to a relatively moderate abrasive wear mechanism.

Micro-ploughing with little micro-cutting and enhanced load sharing made possible by the CNF network are the predominant methods. By limiting excessive plastic deformation and increasing matrix stiffness, the use of CNFs improves wear resistance and decreases material loss. This behavior is in line with results from previous research on carbon nanofiller- reinforced hybrid thermoplastic composites, where increased tribological performance is attributed to improved interfacial adhesion and tribo-film formation [46-48].

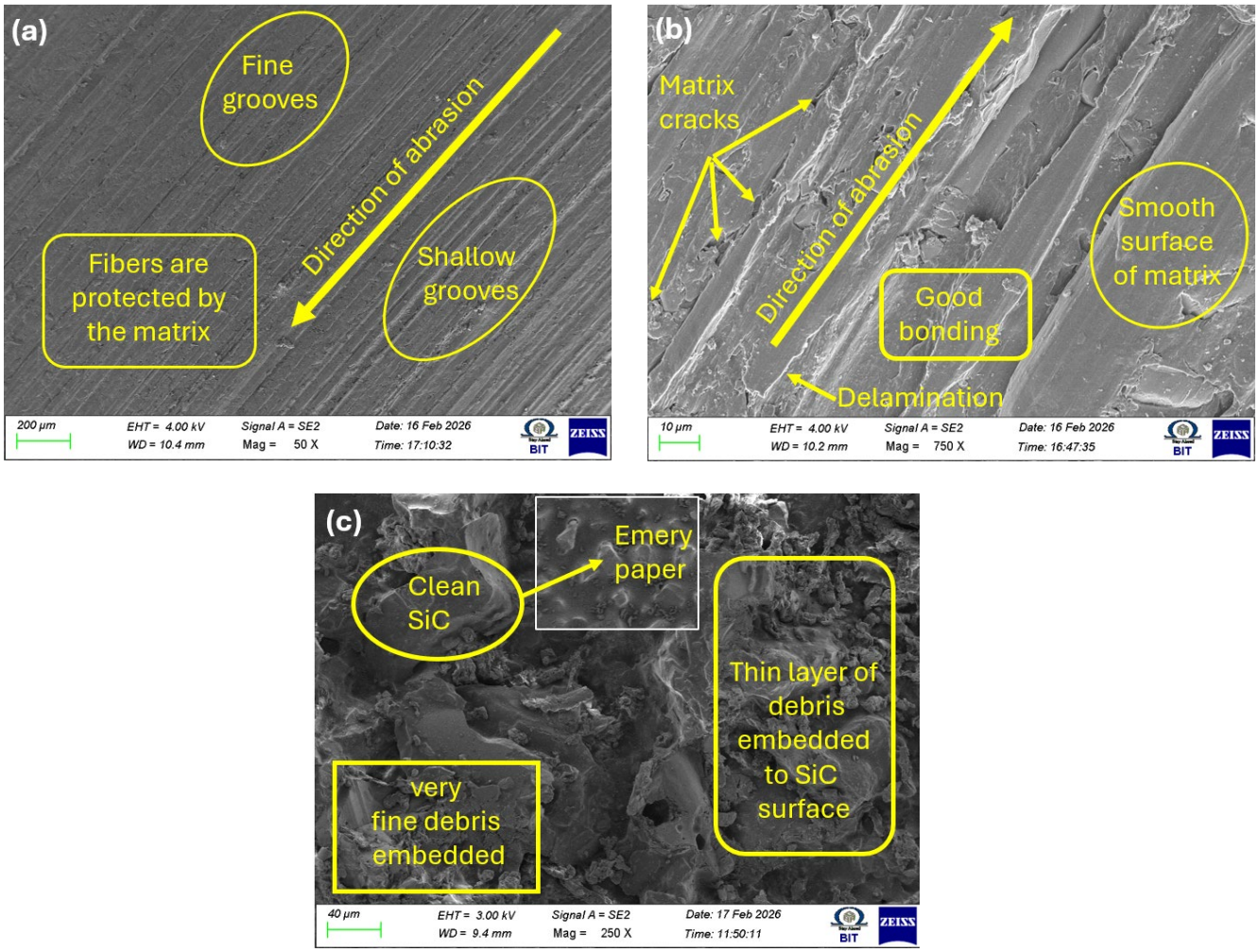

Figure 16: Worn surface micrographs of 0.4 wt% CNF modified GF/PPS composites: (a) 50 X, (b) 250 X, (c) Emery paper used.

Figs. 17a and 17b show that the 0.8 wt% CNF reinforced GF/PPS composite (C2) has the most refined and least damaged surface of all the compositions. While the higher magnification image (Fig. 17b) confirms strong interfacial adhesion and effective stress transfer between the matrix and reinforcement, the low-magnification micrograph (Fig. 17a) reveals a much smoother surface with minimal groove depth, indicating superior resistance to abrasive penetration. It is evident that there is a consistent and stable tribo-layer that serves as a barrier to prevent direct contact with abrasive particles. A more regulated material removal procedure is also suggested by the existence of compacted layers and fine wear debris. The contact mechanism resulting in improved wear characteristics is further supported by Fig. 17c, which depicts the SiC abrasive surface. However, small microcracks are seen in some isolated areas, which could be related to CNF agglomeration at increased filler concentration.

The creation of a persistent protective tribo-film and efficient load bearing by the CNF network and glass fibers support these surface features, which show that the primary wear mechanisms shift towards micro-polishing and mild ploughing. The better interfacial bonding, greater matrix stiffness and hardness, and crack-bridging effects provided by the nanofibers are the main causes of C2's improved performance. Additionally, the formation of a solid third-body layer minimizes wear by reducing direct abrasive contact. These results are in line with current research on hybrid nanocomposites, where a higher nanofiller content improves wear resistance; however, filler agglomeration may cause minor brittleness and localized flaws [49-51].

The evolution of worn surface properties and associated wear mechanisms in GF/PPS hybrid nanocomposites with increasing CNF concentration is summarized in Tab. 11. Deep grooves, widespread fiber pull-out, and matrix smearing are signs of severe surface degradation in the unfilled composite (C0), showing predominant micro-cutting and ploughing mechanisms that lead to subpar tribological performance. Surface degradation is lessened with the addition of 0.4 wt% CNFs (C1), resulting in narrower grooves and better integrity. Moderate performance results from the wear process shifting to mild abrasion with partial tribo-film development, which reflects improved interfacial bonding and load-sharing capabilities.

A smooth surface with a stable and consistent tribo-layer is seen at increased CNF loading (C2, 0.8 wt%). In order to minimize material removal, the primary mechanism changes to micro-polishing with protective layer creation. This leads to better overall performance and wear resistance. According to published research on thermoplastic hybrid

nanocomposites, these results verify that CNF reinforcement successfully changes the wear mechanism from severe abrasive damage to controlled mild wear.

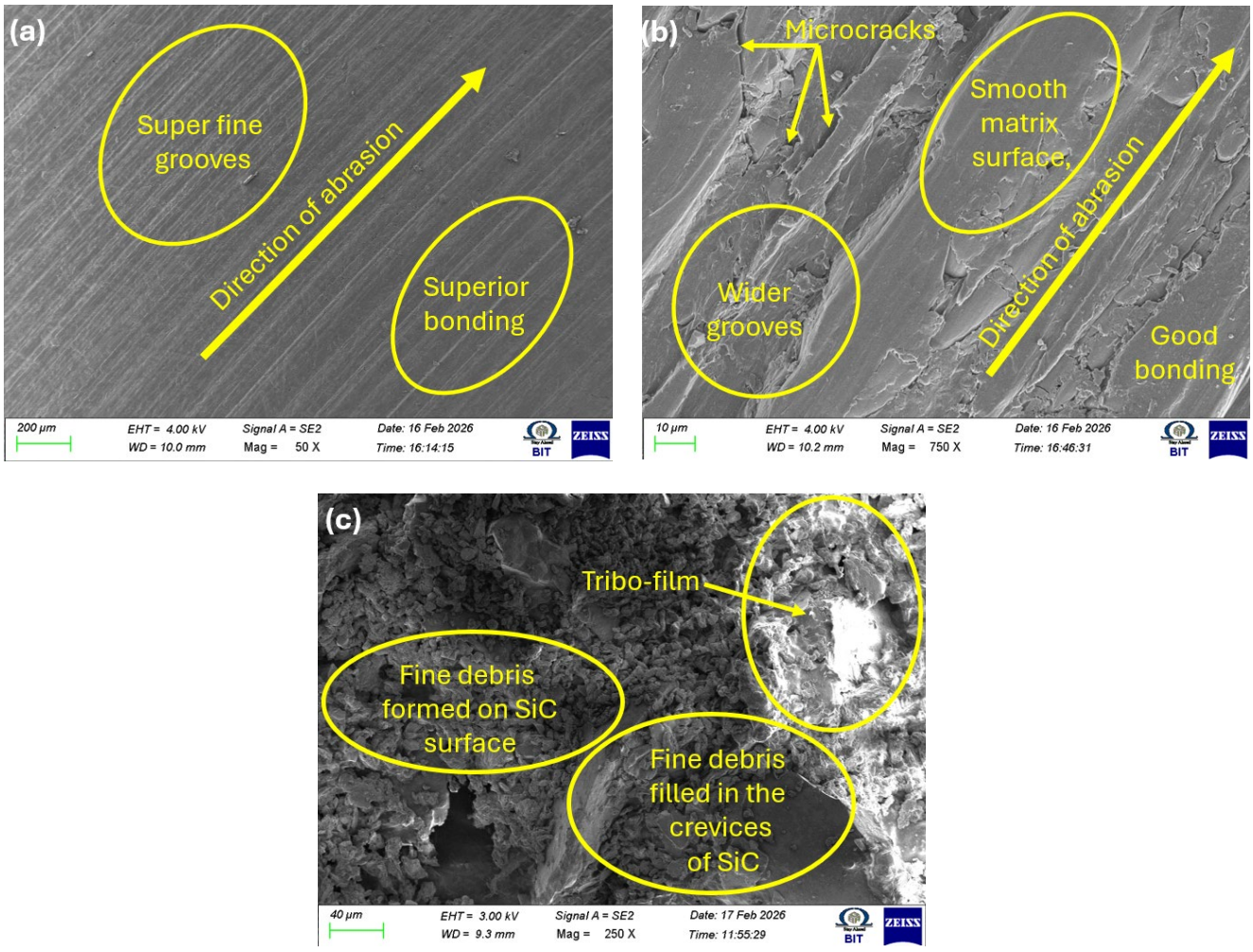

Figure 17: Worn surface micrographs of 0.8 wt% CNF modified GF/PPS composites: (a) 50 X, (b) 250 X, (c) Emery paper used.

Composite	Surface Features	Dominant Wear Mechanisms	Performance
C0	Deep grooves, extensive fiber pull-out, matrix smearing	Severe micro-cutting and ploughing	Poor
C1	Shallower grooves, reduced surface damage	Mild abrasion with partial tribo-film formation	Moderate
C2	Smooth surface, stable and uniform tribo-layer	Micro-polishing with protective layer formation	Best

Table 11: Comparative evaluation of worn surface morphology, dominant wear mechanisms, and tribological performance of GF/PPS/CNF hybrid nanocomposites

Correlation of structure, property, and two-body abrasion

The physicochemical and mechanical properties of GF/PPS/CNF hybrid nanocomposites are closely associated with their enhanced tribological performance. The π–π interactions between CNFs and the PPS matrix are confirmed by FTIR data, suggesting improved interfacial compatibility without changing the chemical structure. Increased density and decreased void content (especially in C2), which reduce defect sites and limit fracture formation during abrasion, are indicative of this enhanced interaction. By enhancing load-bearing capacity and interfacial adhesion, the notable increase in hardness (20%) and ILSS (23.7%) with increased CNF content further contributes to improved wear resistance. Because the strengthened construction prevents micro-cutting and encourages the development of a solid lubricating transfer coating, decreased wear loss and lower CoF are seen. Overall, the reduction in wear loss and CoF is governed by the synergy of improved interfacial bonding, decreased voids, and increased mechanical integrity, with 0.8 wt% CNF (C2) showing the best performance.

CONCLUSION

- The incorporation of carbon nanofibers (CNFs) greatly improved the overall mechanical and tribological performance of GF/PPS hybrid nanocomposites, indicating the usefulness of nanoscale reinforcement in PPS-based structural systems.
- Without changing the intrinsic chemical structure of PPS, FTIR study verified enhanced interfacial contacts between CNFs, glass fibers, and the PPS matrix, suggesting that the reinforcement process is primarily physical.
- By increasing density, decreasing vacancy content, increasing hardness, and improving interlaminar shear strength, the addition of CNFs enhanced the mechanical and physical integrity of the composites, which in turn led to better load transfer and stronger fiber–matrix adhesion.
- Tribological studies showed that CNF reinforcement successfully decreased wear loss and coefficient of friction; the 0.8 weight percent CNF-filled composite performed best because a continuous and stable lubricating tribo-film was formed.
- Sliding velocity and SiC grit size were the most important parameters influencing wear loss, while applied load mostly affected the coefficient of friction, according to statistical ANOVA data, underscoring the considerable dependency of abrasive wear behavior on operating conditions.
- The developed regression models demonstrated good predictive capability and strong agreement with experimental data, confirming their appropriateness for precise wear and friction behavior prediction within the studied design space.
- The wear mechanism changed from severe micro-cutting, matrix degradation, and fiber debonding in unfilled composites to relatively mild ploughing, micro-polishing, and protective tribo-layer creation in CNF-filled composites, according to worn surface morphology.
- Better wear resistance and friction stability were a result of the combined effects of increased hardness, better interfacial bonding, fewer defects, and stable tribo-film formation.
- The fabricated CNF-reinforced GF/PPS hybrid nanocomposites exhibit great promise for automotive transmission parts, gears, bearing cages, thrust washers, and aerospace sliding assemblies operating under harsh tribological environments due to their enhanced hardness, interfacial strength, and superior abrasion resistance.
- The current work is constrained to dry abrasive wear conditions and a narrow range of CNF concentration under laboratory-scale testing, notwithstanding the encouraging outcomes. The performance under lubricated and high-temperature working circumstances, environmental aging resistance, and long-term durability were not examined. To further enhance the suitability of these composites for next-generation lightweight moving components, future research should concentrate on fatigue–tribology interaction, high-temperature and lubricated wear behavior, environmental stability, and multi-scale optimization of CNF dispersion using hybrid solid lubricants like graphene and MoS_2.

REFERENCES

[1] Stankiewicz, K., Lipkowski, A., Jędral, A., Bona, A., Kowalczyk, P. (2025). Processing opportunities for glass fiber reinforced polyphenylensulfide (PPS) composite recyclate, Compos. Part A Appl. Sci. Manuf., 199, pp. 109192, DOI: https://doi.org/10.1016/j.compositesa.2025.109192.

[2] L., Yu, Y., Huang, H., Yin, X., Peng, J., Sun, J., Huang, L., Tang, Y., Wang, L. (2019). High-performance polyphenylene sulfide composites with ultra-high content of glass fiber fabrics, Compos. Part B Eng., 174, pp. 106790, DOI: https://doi.org/10.1016/j.compositesb.2019.05.001.

[3] Yuan, W., Yao, X., Guo, Q., Li, C., Chi, B., Yu, J. (2024). Tribological Performance of Shaft and Surface Pairs with PPS and its Composites in Seawater under Cyclic Loading, Tribol. Lett., 72(3), pp. 1–19, DOI: https://doi.org/10.1007/s11249-024-01901-0.

[4] Friedrich, K. (2018). Polymer composites for tribological applications, Adv. Ind. Eng. Polym. Res., 1(1), pp. 3–39, DOI: https://doi.org/10.1016/j.aiepr.2018.05.001.

[5] Holmgren, J., Kassman, Å., Lindgren, J. (2024). The influence from PTFE on surface and sub-surface damages of glass fiber reinforced PPS, Tribol. Int., 194, pp. 109520, DOI: https://doi.org/10.1016/j.triboint.2024.109520.

[6] Li, J., Liang, M., Zhao, X., Zhou, S., Zou, H. (2025). Assessing the Influence of Inorganic Nanoparticles on the Mechanical and Tribological Performance of PPS-Based Composites: A Comparative Study, Polymers (Basel)., 17(19), DOI: https://doi.org/10.3390/polym17192573.

[7] Dabees, S., Wickramasingha, Y.A., Dharmasiri, B., Austria, E., Akhavan, B., Hayne, D.J., Henderson, L.C. (2024). Tribological behaviour of surface modified carbon-fibre-reinforced polyphenylene sulphide under dry condition, Tribol. Int., 194(3), pp. 109528, DOI: https://doi.org/10.1016/j.triboint.2024.109528.

[8] Sahu, S. K., & Rama Sreekanth, P. S. (2024). Multiscale RVE modeling for assessing effective elastic modulus of HDPE based polymer matrix nanocomposite reinforced with nanodiamond. International Journal on Interactive Design and Manufacturing (IJIDeM), 18(9), pp. 6371-6380.
[9] Sahu, S. K., Sreekanth, P. R., Saxena, K. K., & Ma, Q. (2024). Effect of graphene reinforcement on the tensile and flexural properties of thermoplastic polyurethane nanocomposite using experimental and simulation approach. Advances in Materials and Processing Technologies, pp. 1-17.
[10] Badgayan, N. D., Sahu, S. K., & PS, R. S. (2020). Investigation of wetting behavior of HDPE reinforced with nanoscopic 1D/2D filler system using contact angle goniometry. Materials Today: Proceedings, 26, pp. 331-334.
[11] Srinivas, S., Hemanth, R., Harshavardhan, B., Ananthapadmanabha, G.S., Suresha, B. (2024). Effect of Surface Treated Nanofillers on Abrasive Wear of Carbon Fiber/Polyamide Blend Composites, Tribol. Ind., 46(4), pp. 664–76, DOI: https://doi.org/10.24874/ti.1719.07.24.09.
[12] Meftahi, A., Sabery, M., Alibakhshi, S., Walsh, M., Bechelany, M., Youssef, A., Barhoum, A. (2025). Carbon nanotubes and nanofibers as building blocks for the future: Structure, synthesis, properties, and functionalization perspectives, Mater. Sci. Eng. B, 322, pp. 118622, DOI: https://doi.org/10.1016/j.mseb.2025.118622.
[13] Xiao, C., Tan, Y., Wang, X., Gao, L., Wang, L., Qi, Z. (2018). Study on interfacial and mechanical improvement of carbon fiber/epoxy composites by depositing multi-walled carbon nanotubes on fibers, Chem. Phys. Lett., 703, pp. 8–16, DOI: https://doi.org/10.1016/j.cplett.2018.05.012.
[14] Panin, S. V., Alexenko, V.O., Buslovich, D.G. (2022). High Performance Polymer Composites: A Role of Transfer Films in Ensuring Tribological Properties—A Review, Polymers (Basel), pp. 975, DOI: https://doi.org/10.3390/polym14050975.
[15] Kumar, N.H., Adarsha, H., Keshavamurthy, R., Kumar, G. ~L. A. (2024). Influence of Carbon Nano Fibres on Friction and Wear Characteristics of Polymer Composites Synthesized by Fused Deposition Modelling, J. Inst. Eng. Ser. D, DOI: https://doi.org/10.1007/s40033-024-00747-z.
[16] Zaghloul, M.M.Y., Steel, K., Veidt, M., Martin, D., Firouzi, M., Heitzmann, M.T. (2023). Influence of Counter-Face Grit Size and Lubricant on the Abrasive Wear Behaviour of Thermoplastic Polymers Reinforced with Glass Fibres, Tribol. Lett., 71(3), pp. 102, DOI: https://doi.org/10.1007/s11249-023-01774-9.
[17] Jain, A., Somberg, J., Emami, N. (2019). Development and Characterization of Multi-Scale Carbon Reinforced PPS Composites for Tribological Applications, Lubricants, pp. 34, DOI: https://doi.org/10.3390/lubricants7040034.
[18] Shivamurthy, A., Boranna, R., Jagannat, R., Prashanth, G., Bheemappa, S., S M, D. (2024). Mechanical Properties and Analysis of Two-body Abrasive Wear Behaviour of Graphene Modified Carbon/Epoxy Composites Using Taguchi's Technique, Tribol. Ind., 46, pp. 66–79, DOI: https://doi.org/10.24874/ti.1512.07.23.09.
[19] Umesh, G.L., Rudresh, B.M., Krishnaprasad, N.J., Madhu, D. (2022). Micro fillers effect on two body abrasive wear behavior of Polyamide 66, Polyamide 6 blendbased composites, Mater.Today Proc., 54, pp. 217–222, DOI: https://doi.org/10.1016/j.matpr.2021.08.296.
[20] Rajashekaraiah, H., Bheemappa, S., Yang, S.-H., Mohan, S. (2016). Abrasive wear behaviour of thermoplastic copolyester elastomer composites: A statistical approach, Int. J. Precis. Eng. Manuf., 17(6), pp. 755–763, DOI: https://doi.org/10.1007/s12541-016-0093-x.
[21] Ahmad, S.M., Channegowda, G.M., Shettar, M., Bhat, A. (2025). Comparative Analysis and Predictive Modeling of Wear Performance of Glass- and Bamboo Fiber-Reinforced Nanoclay–Epoxy Composites Using RSM and ANN, Polymers (Basel), pp. 3286, DOI: https://doi.org/10.3390/polym17243286.
[22] Sanman, S., Manjunath, A., Prashanth, K.P., Shadakshari, R., Sunil, S.K. (2023). An experimental study on two body abrasive wear behavior of natural fiber reinforced hybrid polymer matrix composites using Taguchi analysis, Mater. Today Proc., 72, pp. 2021–2026, DOI: https://doi.org/10.1016/j.matpr.2022.07.400.
[23] Wang, L., Kelly, P. V., Ozveren, N., Zhang, X., Korey, M., Chen, C., Li, K., Bhandari, S., Tekinalp, H., Zhao, X., Wang, J., Seydibeyoğlu, M.Ö., Alyamac-Seydibeyoglu, E., Gramlich, W.M., Tajvidi, M., Webb, E., Ozcan, S., Gardner, D.J. (2023). Multifunctional polymer composite coatings and adhesives by incorporating cellulose nanomaterials, Matter, 6(2), pp. 344–372, DOI: https://doi.org/10.1016/j.matt.2022.11.024.
[24] Bheemappa, S., Ramesh, B.N., Subbaya, K.M., Kumar, B., G., C. (2010). Influence of graphite filler on two-body abrasive wear behaviour of carbon fabric reinforced epoxy composites, Mater. Des., 31, pp. 1833–1841, DOI: https://doi.org/10.1016/j.matdes.2009.11.006.
[25] M R, H., Pal, B., R, K., S P, S. (2025). Influence of MoS2 nano-filler additions on wear behavior of carbon fiber reinforced epoxy composites, Adv. Compos. Mater., 34(1), pp. 34–48, DOI: https://doi.org/10.1080/09243046.2024.2352895.
[26] Dhanola, A. (2023). A comprehensive overview on tribo-mechanical characteristics of hybrid plant fiber–based biocomposites, Emergent Mater., 6(6), pp. 1707–1726, DOI: https://doi.org/10.1007/s42247-023-00567-z.
[27] Mohan, R., Daniel James D, J., Mohan, S., Panneerselvam, K. (2025). Evaluation and study of PBI reinforced with HDPE on abrasive wear using ANOVA and CODAS approach for protective shell applications, J. Pipeline Sci. Eng., 6, pp. 100279, DOI: https://doi.org/10.1016/j.jpse.2025.100279.

[28] B., H., Ravishankar, R., Dixit, A., Anandraj, D. (2024). Tribological Behaviour of Short Carbon Fiber Reinforced Polyethersulfone Composites with PTW Filler, Tribol. Ind., 46, pp. 217–235, DOI: https://doi.org/10.24874/ti.1532.08.23.10.
[29] Bhanavase, V., Jogi, B., Dama, Y. (2025). Wear behavior study of glass fiber and organic clay reinforced poly-phenylene-sulfide (PPS) composites material, Obrab. Met., 27(1), pp. 203–217, DOI: 10.17212/1994-6309-2025-27.1-203-217.
[30] ASTM International, Standard test methods for density and specific gravity (relative density) of plastics by displacement (ASTM D792-20) (2020), West Conshohocken, PA. DOI: https://doi.org/10.1520/D0792-20.
[31] ASTM International, Standard test method for rubber property—durometer hardness (ASTM D2240-15e1), (2015) ASTM International, West Conshohocken, PA.
[32] ASTM International, ASTM D2344/D2344M-22: Standard test method for short-beam strength, ASTM International (2022). DOI: https://doi.org/10.1520/D2344-D2344M-22.
[33] Thwe, M. M., & Liao, K. (2002). Durability of bamboo-glass fiber reinforced polymer matrix hybrid composites. Compos. Sci. Technol., 62(3), pp. 375–387, DOI: https://doi.org/10.1016/S0266-3538(01)00184-7
[34] Taguchi, G. (1990), Introduction to quality engineering: Designing quality into products and processes, Asian Productivity Organization.
[35] ASTM International, Standard test method for wear testing with a pin-on-disk apparatus (ASTM G99-17), ASTM International (2017). DOI: https://doi.org/10.1520/G0099-17.
[36] Montgomery, (2020) D.C., Design and analysis of experiments, 10th ed., Wiley.
[37] Chen, J., Liu, B., Gao, X., Xu, D. (2018). A review of the interfacial characteristics of polymer nanocomposites containing carbon nanotubes, RSC Adv., 8(49), pp. 28048–28085, DOI: https://doi.org/10.1039/C8RA04205E.
[38] Li, N., Li, X., Yao, A., Guo, Z., Liu, X., Li, H., Wang, Y., Liang, J., Chen, Z. (2025). Effect fiber length on mechanical and thermal properties of glass fiber reinforced polyphenylene sulfide composite, J. Reinf. Plast. Compos., 44(15–16), pp. 902–912, DOI: https://doi.org/10.1177/07316844241232960.
[39] Li, Y., Wang, Q., Wang, S. (2019). A review on enhancement of mechanical and tribological properties of polymer composites reinforced by carbon nanotubes and graphene sheet: Molecular dynamics simulations, Compos. Part B Eng., 160(October 2018), pp. 348–361, DOI: https://doi.org/10.1016/j.compositesb.2018.12.026.
[40] Demir, M.E., Cetkin, E., Ergün, R.K., Denizhan, O. (2024). Tribological and mechanical properties of nanofilled glass fiber reinforced composites and analyzing the tribological behavior using artificial neural networks, Polym. Compos., 45(5), pp. 4233–4249, DOI: https://doi.org/https://DOI.org/10.1002/pc.28055.
[41] Li, Y., Huang, X., Zeng, L., Li, R., Tian, H., Fu, X., Wang, Y., Zhong, W. (2019). A review of the electrical and mechanical properties of carbon nanofiller-reinforced polymer composites, J. Mater. Sci., 54, DOI: https://doi.org/10.1007/s10853-018-3006-9.
[42] Siengchin, S. (2011). Carbon Nanofiber Reinforced and PU-toughened POM Ternary Composites: Friction, Wear and Creep Properties, Mech. Eng. Res., 1(1), pp. 69–78, DOI: https://doi.org/10.5539/mer.v1n1p69.
[43] SJ, P., SH, I., JR, L., JM, R. (2006). Thermal, Frictional and Wear Behavior of Carbon Nanofiber/Poly (methyl methacrylate) Composites, Polym. Soc. Korea, 30(5), pp. 385–390.
[44] Panin, S. V., Kornienko, L.A., Alexenko, V.O., Buslovich, D.G., Bochkareva, S.A., Lyukshin, B.A. (2020). Increasing Wear Resistance of UHMWPE by Loading Enforcing Carbon Fibers: Effect of Irreversible and Elastic Deformation, Friction Heating, and Filler Size, Materials (Basel)., 13(2), DOI: https://doi.org/10.3390/ma13020338.
[45] Shi, Y., Feng, X., Wang, H., Lu, X. (2008). The effect of surface modification on the friction and wear behavior of carbon nanofiber-filled PTFE composites, Wear, 264, pp. 934–939, DOI: https://doi.org/10.1016/j.wear.2007.06.014.
[46] Praveen, B. A. (2026). Mechanical and morphological evaluation of jute fiber reinforced epoxy composites for sustainable structural and automotive applications. Fracture and Structural Integrity, 20(76), pp. 1-16. DOI: https://doi.org/10.3221/IGF-ESIS.76.01
[47] Jain, A., Somberg, J., Emami, N. (2019). Development and Characterization of Multi-Scale Carbon Reinforced PPS Composites for Tribological Applications, Lubricants, pp. 34, DOI: https://doi.org/10.3390/lubricants7040034.
[48] El-Tayeb, N.S.M. (2009). Two-body abrasive behaviour of untreated SC and R-G fibres polyester composites, Wear, 266(1–2), pp. 220–232, DOI: https://doi.org/10.1016/j.wear.2008.06.018.
[49] Kumar, S., Singh, K.K. (2020). Tribological behaviour of fibre-reinforced thermoset polymer composites: A review, Proc. Inst. Mech. Eng. Part L J. Mater. Des. Appl., 234, pp. 146442072094155, DOI: https://doi.org/10.1177/1464420720941554.
[50] Singh, S.K., Singh, L.D., Vijay, K., Sonker, P.K., Verma, Y.K. (2026). Improved Mechanical and Tribological Performance of GFRP Laminate Composites with TiO 2–SiC Hybrid Fillers in Modified Epoxy Matrix for Automotive Applications, Polym. Compos., 47(5), pp. 4246–4260, DOI: https://doi.org/https://doi.org/10.1002/pc.70422.

[51] Chan, J.X., Wong, J.F., Petrů, M., Hassan, A., Nirmal, U., Othman, N., Ilyas, R.A. (2021). Effect of Nanofillers on Tribological Properties of Polymer Nanocomposites: A Review on Recent Development, Polymers (Basel), pp. 2867, DOI: https://doi.org/10.3390/polym13172867.

[52] Srinivas, S., Hemanth, R., B., H., Ananthapadmanabha, G.S., Bheemappa, S. (2024). Effect of Surface Treated Nanofillers on Abrasive Wear of Carbon Fiber/Polyamide Blend Composites, Tribol. Ind., 46, pp. 664–676, DOI: https://doi.org/10.24874/ti.1719.07.24.09.

[53] Xu, S., Tangpong, X.W. (2013). Tribological behavior of polyethylene-based nanocomposites, J. Mater. Sci., 48, pp. 578–97.

[54] Ramesh, M., Kumar L, R., N., S., Kumar, D., Devarajan, B. (2022). Influence of filler material on properties of fiber-reinforced polymer composites: A review, E-Polymers, 22, pp. 898–916, DOI: https://doi.org/10.1515/epoly-2022-0080.

[55] Gurumurthy, H., Bheemappa, S., Hemanth, R. (2019). The effect of hexagonal boron nitride on wear resistance under two and three-body abrasion modes of polyetherketone composites, Surf. Topogr. Metrol. Prop., 7, pp. 45019, DOI: https://doi.org/10.1088/2051-672X/ab500b.